Dear Editor, dear Reviewers,

we thank the editor and both anonymous referees for their constructive comments. We have addressed all of them in the following point-to-point rebuttal letter and we incorporated the changes in a revised manuscript.
Specifically, we have added additional information in the introduction to emphasize the importance of the possible future consequences of the observed salt karst processes in Solotvyno. Furthermore, we have shortened the geological background, as suggested, and we have combined it with the description of the mining activity. We also reduced the general description of the methodology section and gave additional explanation of SAR data processing. We also included a new section, devoted to analytical modeling to adequately disclose the relation between observed subsidence and mining, geological conditions. We believe that the additional information and investigations foster the better understanding of the significant risk in the area.

the Authors

We thank both anonymous reviewers for their constructive comments. We have addressed all of them in the following point-to-point rebuttal and we will incorporate the changes in the revised manuscript.
As comments by the reviewers have some common remarks, we have sorted each reviewer's comments and grouped those that have common themes.

We marked our responses in blue, in detail (we also uploaded this document as supplementary material, since we couldn't set font color in the interactive comment).

Reviewer 1, General comments: The paper uses InSAR to analyse surface deformation in an area of sinkholes formed due to salt mining in Solotvyno (Ukraine). The major results of the paper are: 1. two velocity maps and time series of LOS displacements, one in the ascending and the other in the descending Sentinel-1 tracks, for the years 2014-2019, with maximum LOS velocities of 5 cm/y. 2. Decomposition of the LOS displacements to vertical and E-W horizontal components. 3. Recognition of linear trends of deformation (no acceleration nor deceleration). The paper is local and mostly technical, showing some interesting results, however, it does not make any attempt to discuss these results, their implications, or their contribution to our general understanding of sinkhole-related processes.

Reviewer 2, General comments: This manuscript applied InSAR to detect ground deformation related to salt extraction-caused sinkholes in Solotvyno (Ukraine). Both ascending and descending datasets from Sentinel-1 satellite were used to decompose horizontal and vertical displacement. Results found that the maximum LOS deformation is 5 cm/yr and the vertical deformation is much more dominant in the area. However, the aim of this paper is not completely clear: are the authors willing to prove the usefulness of InSAR applied to sinkhole deformation (focus on the methodology) or are they interested on the ground deformations detected on the salt mines (focus on the case studies)?

We agree with the reviewers for pointing out that the motivation of the paper is not fully clear. In the past decades satellite radar interferometry has become a widespread tool to detect subtle surface changes, like ground subsidence associated with sinkhole generation. The numerous studies available for the Dead Sea region clearly confirms that. With the advent of coordinated Earth observation, the near real time mapping of surface deformation processes become available. The recent paper by Nof et al. (2019) describes a semi-automatic early warning system that detects precursory subsidence before sinkhole collapse primary based on SAR dataset.

Our study area is not investigated as thoroughly as the Dead Sea region, but it is also severely affected by sudden sinkhole collapses. Collapse of subsurface caverns in the past resulted in dolines, temporally filled with brine and have a size of 150-230 m in diameter. Although today it can be handled as a local problem, it will definitely become a serious issue in the future as the water infiltration caused sinkhole development will propagate through the boundary of the mining area and endanger inhabited areas. Some parts of the city have already been evacuated. Besides the economic losses, the ecologic impact of migrating salt water into underground fresh water system can be catastrophic, which can lead to a regional problem. Recognizing the situation, the European Commission devoted considerable funds to support risk reduction in the area.

The latest sinkhole collapse happened before the launch of the Sentinel-1 mission. Although the issue is well-known, no dedicated terrestrial monitoring network has been installed yet. Therefore, Sentinel-1 satellite interferometry seems to be the only opportunity to support the early identification of areas prone to sinkhole occurrence.

We also agree with the reviewers that a thorough discussion of the results is needed to improve the paper, providing more insight into the mechanisms responsible for sinkhole growth in the area. Although the observed deformation pattern is sparse (Reviewer 1 also noted this regarding the cumulative displacement profiles in comment 6) we tried to perform an inversion to get some information about the dislocation sources. This investigation will be incorporated into the revised version of the ms.

Source modeling

We modeled the deformation observed by InSAR in order to better understand the mechanisms responsible for the sinkhole growth, and constrain the location and depth of underground cavities which can result in sinkhole collapse in the future. The cavity deflation was modeled using rectangular dislocation sources (Okada, 1992; Segall, 2010) within a homogeneous and isotropic elastic half-space. We used a rectangular pressurized crack model, since deformations are presumably related to the destruction of abandoned mines. Despite their simplicity and the inherited approximations, analytical formulations are convenient to model and explain deformation patterns described by a few model parameters. The elasticity assumption implies that the half-space obeys Hooke's law, therefore displacements are considered infinitely small compared to the characteristic size of source dimensions (Lisowski, 2007). The observed gradual subsidence also supports the assumption of pure elastic deformation.

Unfortunately, no reliable information is available on the exact position, extension, orientation and depth of the mining underground. The estimated depth of underground mines varies between 50 m to 400 m, from the center to the perimeter of the mining area. The approximate location of the mines was estimated based on the available maps. We fit simple Okada rectangular dislocation models to the InSAR data using a grid-search method to estimate the initial model parameters. These were refined in a second step based on a Bayesian inversion.

Forward modeling

The coarse estimation of model parameters was accomplished by forward modeling varying source model parameters on a predefined interval. The parameter space of the dislocation models was constrained based on the rough location, geometry and orientation of underground mines available on maps as well as the approximate depth of salt layer. Lack of coherence, either due to change in ground cover or high rate of deformation, does not allow to retrieve the entire deformation pattern associated with sinkhole evolution. Therefore, cumulative deformations from ascending and descending satellite passes covering the same time period, were utilized simultaneously to increase the reliability of source model parameter estimation. The lack of deformation signal around the center of the area of interest makes it difficult to identify the number of source models required to explain the subsidence pattern. We made an exhaustive search for the best-fitting models using the misfit function $\delta = \left[\sum_{i=1}^{N}\sum_{j=1}^{M}\left(d_i - d_{i,m_j}\right)^2/N\right]^{1/2}$, where N is the total number of measurement points, M is the number of source models, d_i is the observed cumulative surface deformation and d_{i,m_j} is the modeled deformation from the j[th] source model projected onto the satellite LoS. Our results suggest a quad-source configuration of subsurface cavities, the model parameters are provided in Tabl. 1.

Source parameter estimation based on Bayesian inversion

To refine the source parameters and estimate associated uncertainties we performed a Bayesian probabilistic inversion (Bagnardi & Hooper, 2018). We modified the open-source GBIS (Geodetic Bayesian Inversion Software, http://comet.nerc.ac.uk/gbis/) code to handle custom source models of multiple rectangular dislocations. We also jointly inverted the cumulative ascending and descending InSAR data to determine deformation source parameters, i.e. horizontal dimensions and horizontal coordinates of rectangular source, depth of dislocation, strike angle of horizontal edge with respect to the North and opening of model (related to volume change), for every models in a single run. Within a Bayesian inversion approach the characterization of posterior probability density functions (PDFs) of source model parameters are accomplished by taking into account uncertainties in the data. The optimal set of source parameters can be extracted from the posterior PDF by finding the maximum a posteriori probability solution. The PDFs of source model parameters are determined from the likelihood function of the residuals between the observations and the model prediction weighted with the inverse of the variance-covariance matrix of the observations. The Bayesian inversion approach requires to quantify errors in the data, which are assumed to be multivariate Gaussian with zero mean and covariance matrix. For multiple

independent data sets, the likelihood function can be formulated as the product of the likelihoods of the individual data sets. To increase the numerical efficiency, the GBIS inversion algorithm samples the posterior PDFs through a Markov chain Monte Carlo method, incorporating the Metropolis-Hastings algorithm, with automatic step size selection. For more details we refer to Bagnardi & Hooper (2018).

Noise covariance of individual interferograms has been well studied, the main error sources are the noise caused by the temporally correlated phase decorrelation and the spatially correlated atmospheric phase delay. Since InSAR observations are inherently relative, the additive phase delays make the accuracy of measurements strongly dependent on the distance. There have been several endeavors to provide an error analysis of TS (Time Series) InSAR output (see e.g. Agram & Simons, 2015; Cao et al., 2018 and references therein), however, we followed the method of Parizzi et al. (2020) and estimated the variance-covariance matrix of InSAR data sets experimentally. As Parizzi et al. (2020) points out, short time separated interferograms (supported by Sentinel-1 mission with multi-baseline analysis) are much more dominated by atmospheric propagation delay rather than phase variation due to deformation. After atmospheric phase correction the interferometric measurement error is practically the residual atmospheric phase delay, as short time separated interferograms can be considered deformation-free. The mean variograms of the residual atmospheric phase shows a stationary behavior and can be approximated by a covariance function. Since both deformation and average velocity are related to the phase by a scale factor, the error estimates can be simply computed. We used an exponential covariance model fitted to the data to determine the variance-covariance matrix of deformation in the Bayesian inversion. For both the ascending and descending data sets similar models were obtained with a moderate range values of 2.4 and 2.2 km for the ascending and descending datasets respectively.

Best-fit model parameters obtained from the forward modeling were utilized as starting values for the Bayesian parameter estimation. During the inversion the parameters were allowed to vary within reasonable limits taking into account the geological constrains and information of the mining activity. The optimal model parameters are summarized in Tabl. 1., coordinates are given in a local rectangular coordinate system. Our final model assumes four rectangular-shaped subsurface cavities, developed in the salt layer. One source with a rectangular dislocation (model #1) of size 24.1 m × 64 m is located above the eastern edge of working panels of mine №9 at an estimated depth of 199.7 m. This mine was closed in 2008 due to water inrush. The moderate value of volume change suggests that this depression is an early stage of sinkhole development. The second source model (model #2) lies approximately 400 m southwest far from the first one and has a horizontal dimension of 63.5 m × 187.8 m, the required height change explaining the deformation pattern is -1.2 m. The elongated shape in roughly North-South direction of the source model is in agreement with the subsurface mining activity. Between the main corridors of mines №9 and №10 long working panels were cut with varying length between a few tens to a few hundreds of meters. The third dislocation model (model #3) is located in the western periphery of the area affected by deformations. The model is roughly symmetric with a horizontal side length about 80 m and located at a depth of 273.1 m. There are several shallow mines (numbered by 1 to 5 on Fig. 5. in the ms.) there, established around the 18-19th century. These were

completely destroyed as the numerous, small-scale dolines filled with brine indicate on the surface. The source model parameters suggest that the inverse modeling tried to find a global solution for the observed subsidence pattern. However, a single source is unable to sufficiently explain the complex deformation pattern, a number of near-surface, small-scale voids, related to salt dissolution are needed as well. The fourth source model (model #4) is located beneath the working panels of mine №8, where heavy subsidence occurred around 2010, which resulted in the formation of the twin lakes. The depth of the model is about 296 m, the horizontal extension of the model is 72.3 m × 82.1 m. The estimated opening equals to approximately an 18,000 m^3 volume change. Taking into account the horizontal extension of the existing surface depressions of the nearby twin lakes, 15,000 and 17,000 m^2 respectively, our modeling results seem reasonable. The question whether a new doline will form and will merge with the existing two in the future or the boundary of the area affected by subsidence will expand toward south, requires further observations besides radar interferometry.

Regarding the quantitative analysis of the inversion results Figs. 1. and 2. shows the LoS deformation determined from the best-fitting quad-configuration source model, the Sentinel-1 cumulative LoS deformations as well as the difference between the observed and modeled values, for both the ascending and descending passes respectively. It can be assessed that the main features of the subsidence pattern on the northern and southern periphery are reasonably well captured by the source models. However, the modeled deformation on the western part of the area does not fit to the observations, especially when comparing to the ascending data set, where modeled deformation overestimates the observed ones. As it was mentioned, under this area the salt layer upwells close to the surface and many small dropout doline have already formed and a single source model cannot adequately explain the surface deformation pattern.

Apart from larger discrepancies at some individual points the modeled deformation pattern fit well to the observed ones. However, it has to keep in mind when evaluating the inversion performance that it wasn't possible to properly sample the deformation pattern with InSAR, only the margins of the area was mapped adequately. Due to the sparse InSAR observation distribution in the middle of the area, we could not fit a proper source model there, which can be seen immediately when inspecting the modeled and observed deformations along selected profiles given on Fig. 3. Regarding the ascending data set, the same North-South oriented profile was used to check the model fit to InSAR observations as shown Fig. 10. (in the original ms.) to check the subsidence evolution in time. In the northern part (starting from point A to appr. 200 m) of the cross-section the source models are capable to explain reasonably well the observed deformation. The misfit of the modeled deformation is characterized by a standard deviation (std.) of ± 0.49 cm. However, for the second half of the investigated profile, between 200 and 800 m, the modeled deformation differs significantly from the observed ones. The reason for the large discrepancies in the middle of the cross-section comes from that, that it was not possible to find a proper source model based on the very scarce InSAR observations in the center of the area. On the southern edge of the cross-section (between 700 and 800 m) the applied single source model is not capable to resolve the observed deformation. Probably the InSAR derived deformations reflect the effect of

more than a one subsurface cavern. The bottom figure of Fig. 3. shows the observed and modelled deformations on a roughly east-westward cross section (the location of the section is the same as for Fig. 11. in the original ms.). Modeled deformation shows a reasonably sufficient fit to the InSAR deformations. The misfit of the model is characterized by a ± 1.87 cm std. The magnitude of the observed deformation is adequately described by the model, however, the location of extremities is a slightly miss-estimated. The profile crosses the area in the North, where model #1 and model #2 is located. The effect of the two source models can be separated on the modeled deformations. Of course, the fine details revealed by InSAR observations cannot be reproduced by analytical modeling. Despite of the simple formulas, analytical models can produce reasonable first-order results of the subsurface processes. However, the possible interaction between the sources were not considered. As Pascal et al. (2013) points out, superposition of analytical models requires attention for adjacent models.

Reviewer 1, specific comment 1. The geographical and geological background is far too long and detailed and is mostly irrelevant to the scope of the paper. The background sentences in the introduction are sufficient to understand the setting.

Reviewer 2, specific comment 1. The authors talked a lot about geological settings in Section 2 “Geographical and geological background”, but it looks not related to your discussions later in the paper. The same problem as in Section 3. Could you relate your deformation results to the geological settings and mining activities? Maybe you can add a section in discussion to talk about the relationship between deformation and geological setting/ mining activities.

We agree with the reviewers that the given geological background is too lengthy in the present form. Our aim was to summarize the information available for the region, since most of the papers, textbook and maps are difficult to acquire and mostly written using the Cyrillic alphabet. We will shorten this section in the revised version of the ms. and add the results of the analytical source modeling to link the surface processes with geology and past mining activity.

Reviewer 1, specific comment 2. Materials and methods: lines 153-169 and 190-199 are introductory and background descriptions and should not appear in this section. Only lines 170-187 and 200-229 are relevant and should be combined with lines 53-62 to one section.

Reviewer 2, specific comment 2. In section 4 “Materials and methods”, the first paragraph (line 155-175) is not related to this section, you have to focus on your SAR datasets and what method you developed/used to process your SAR data. My suggestion is to simplify your section 2 and discuss more about your methodology. Describe more about what software you used to process Sentinel-1 data, how do you deal with coherent pixel selection, or maybe how to mitigate atmospheric delay.

We thank the referees this remark. In the revised ms. we will merge the suggested paragraphs for the introduction to Material and methods.

We also will include more details on Sentinel-1 processing in Section 4.2 as follows (from line 221., original text given in black).

The interferograms were generated using the Gamma software (Wegmüller et al., 2016). We considered pairs of four consecutive SAR scenes to include redundancy in the interferogram network, which facilitates reduction of errors. We utilized both phase-stable single scatterers (PS) as well as distributed targets (DS), which ensures long-term coherence. The initial set of PS candidates was selected based on the high temporal stability of the backscattering as well as the low spectral diversity. For the DS scatterers we used multilooking with a factor of 5 x 1 (5 samples in range and 1 in azimuth) to increase signal to noise ratio but keeping in mind the spatial extent of the sinkholes. Distributed targets resulted in a 15 m x 15 m pixel size in the slant range, which enables to detect localized deformation caused by surface depression. The flat-earth phase and topographic phase were removed from the interferograms. In the multi-baseline approach interferograms were unwrapped in space first, finding the unambiguous phase values. The phase unwrapping was accomplished in an iterative way with quality control, keeping those PS and DS pixels for the next step, which satisfy the phase model with reasonably small (< 1 rad) residuals. A two-dimensional phase model involving height corrections relative to the reference model (SRTM heights mapped to radar coordinates) and linear deformation rate was chosen. The residual phase consists of non-linear deformation phase, atmospheric propagation delay, error in the height correction estimates and other noise terms. The spatially correlated, low-frequency part of the residual phase was separated by spatial filtering from the residual phase, since unwrapping residual phase of point differential interferograms is much simpler than unwrapping the original point differential interferograms. The whole process was iterated starting from dividing the area into patches, where the linear phase model approximation was suitable. Using a multi-reference stack based on consecutive SAR scenes, the deformation phase can be kept as small as possible. With the constant refinement of the phase model a single regression was applied on the whole area. The main output of the regression analysis was the unwrapped phase. The various phase terms were summed up and then the unwrapped phases were connected in time and inverted to deformations using a least squares approach minimizing the sum of the square weighted residual phases (Berardino, Fornaro, Lanari, & Sansosti, 2002; Wegmüller et al., 2016). The atmospheric phase and non-uniform deformation phase are present in the time series of unwrapped phases. To discriminate the two, we identified highly deforming areas and excluded those phase values to estimate atmospheric propagation delay. Atmospheric phases were determined as a combination of height dependent atmospheric delay plus the long-wavelength component of the SBAS inverted residual phase. We used a low-pass filter with characteristic length of 5 km. Long-wavelength (> 5 km) non-linear deformation was mapped into atmospheric correction. However, the area affected by subsidence is rather compact so we expect no long-wavelength non-uniform motion.

Reviewer 2, specific comment 3. The description of decomposition method in Section 5.2 should move to the section “Methods”. And in this section, you just need to discuss the decomposition results.

Thank you for the suggestion, we will move the paragraph describing LoS decomposition to Sec. 4. in the revised version of the ms.

Reviewer 1, specific comment 3. The authors present ascending and descending data and claim (line 254) that the “average (descending) deformation rate shows similar pattern as for the ascending pass. This suggests that the deformation consists mostly of vertical component.”. This declaration has not been proved in any way, for example, by a graph comparing all ascending vs descending LOS velocities. Furthermore, similar patterns are not enough to prove that claim, the values should also be close (albeit moderated by the incidence angle). This should be shown.

Reviewer 1, specific comment 5. The vertical velocities are about twice in magnitude (max 40 mm/y) compared to the horizontal velocities (max 20 mm/y). This means that deformation does not consist mostly of vertical deformation and that the horizontal movements should be considered and explained. Furthermore, Fig. 14 and lines 291-292 show that “The northern part of the deforming area clearly shows a westward displacement, whereas its southern part shows displacement towards the east”. This means horizontal movements away from the subsidence centre (the sinkhole), which is counterintuitive, and should be explained and/or discussed.

We agree with the reviewer; the observed deformations must be explained in a coherent way, thanks for the inspiring comment. Considering a pure elastic model, the sketch beneath (please see the supplementary file) shows that the evolution of a depression means deformation not only with vertical component but horizontal as well. The farther a point from the center, the more pronounced is the horizontal deformation, which direction points away from the center of the subsidence bowl. Due to the side looking radar geometry, the observed horizontal deformation is not symmetric. However, asymmetry can also be caused by change in the material property (change in geology).

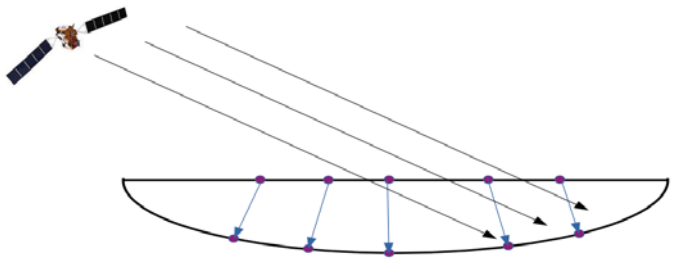

Reviewer 1, specific comment 4. The equation relating LOS to vertical and horizontal components should also include the heading angle between the track and the north.

Reviewer 2, specific comment 4. The equation of decomposition is wrong, the heading angle is missing. please refer to (Fuhrmann & Garthwaite, 2019).

Thank you for the reviewers to point out this issue. Since the North-South deformations are neglected in the decomposition, the azimuth enters only in the East-West term with the factor, cosine of the heading. Taking into account the heading values for S1, this term is about ±0.96 (depending on pass direction), therefore it was neglected. We acknowledge that equation of decomposition can be misleading in the present form, therefore, we will include the original, full 3D expression in the revised version of the ms. with proper citation.

Reviewer 1, specific comment 6. Figures 10 shows a cross sections over an area that is highly incoherent, while the lines are continuous from side to side. The authors should explain how this section was made and make it clear where are the true points and where are the lines based on interpolation.

We agree with the reviewer that it must be emphasized in the ms. that the LoS deformation profiles were constructed by interpolation. We applied a natural neighbor interpolation method based on the points satisfying some distance criteria (< 50 m) around the location of the profile. Therefore, Figs. 10. and 11. show much more the gradual deformation of a zone instead of the single profile. That's the reason we did not mark the location of true points on the deformation curves. This information will be added to the revised ms.
Location of cross-sections was selected to get information in roughly perpendicular directions of the area, it was chosen by visual inspection of point distribution.

Reviewer 1, specific comment 7. Line 183-184: "separation of total line-of-sight (LOS) deformation into east-west and vertical components which can help to understand the mechanism of sinkhole collapse and the progress of underground processes". The authors do not show anywhere later in the paper any insight or discussion regarding the mechanism of sinkhole collapse and progress of underground processes. So what is the motivation for this separation to vertical and horizontal components?

The separation of LoS deformation into vertical and horizontal components involves some spatial averaging to resample both datasets to a common grid, which has a smoothing effect. This can help to suppress possible outliers in one hand, on the other hand it is much easier to interpret horizontal and vertical deformations compared to LoS measurements. We agree with the reviewer, that the interpretation was not satisfactory. To constrain the underground processes, we conducted an analytical modeling described at the beginning of authors' responses.

Reviewer 1, specific comment 8. Lines 257-259: can the authors please explain the large difference between the ascending and descending velocities in the "landslide" area?

We did not investigate deformation pattern related to the landslide in the original ms., since we focused mining-related displacements, which can help the early identification of sinkhole prone areas.

Based on the relief (represented by SRTM model) and some assumptions about the nature of displacement related to landslide, we can conclude the following. Since this investigation is not part of the ms., the figs referred in the text can be found in the supplementary pdf material.

We take the assumption that the direction of motion is along the local direction of steepest descent, which is shown by the surface gradient vector. This condition is routinely applied not only in landslide mapping applications, but also in investigations related to glacier displacement mapping. The horizontal orientation of the gradient vector in the landslide area varies between -1.8 and -2.2 radian (-103°-126°), where angles are measured relative to the East and increases towards to the North. Therefore, the slope is assumed to move towards south with a slight westward motion (see first fig). The magnitude of the gradient vector is shown on the second figure, it is about 22-25%, which suggests a moderately steep slope. Assuming that the vertical deformation is more pronounced than the horizontal (westward) motion, which can be plausible based on the gradient vector, the apparent deformation in the LoS direction for the descending pass is larger (see the sketch on the third fig.), that is the reason for the difference. [The incidence angles are 41.4° and 36.3°, for the ascending and descending passes respectively (see Tabl. 2. of the original ms.).]

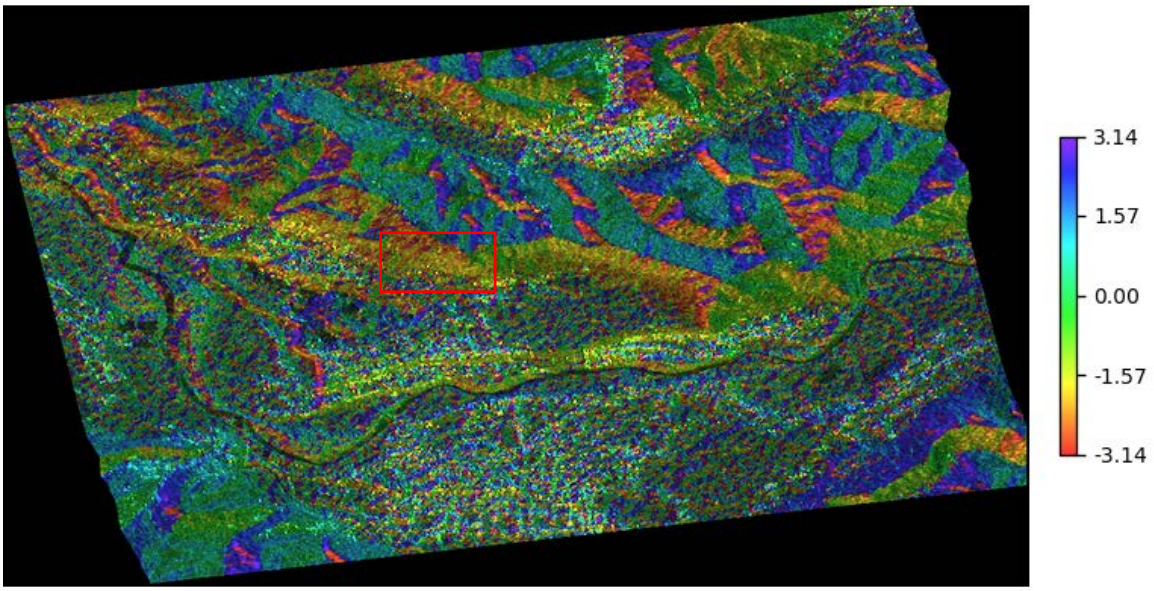

Orientation angle of SRTM gradient vector (values are in radian relative to East, North is π/2, South is –π/2), landslide area is marked by the red box.

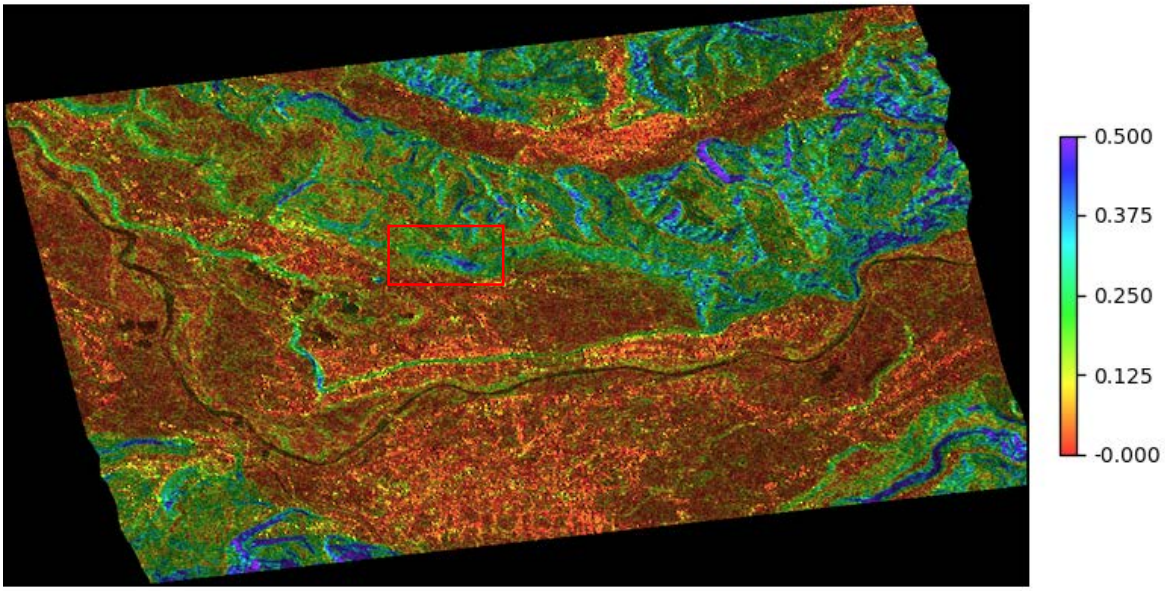

Normalized magnitude of the SRTM gradient vector.

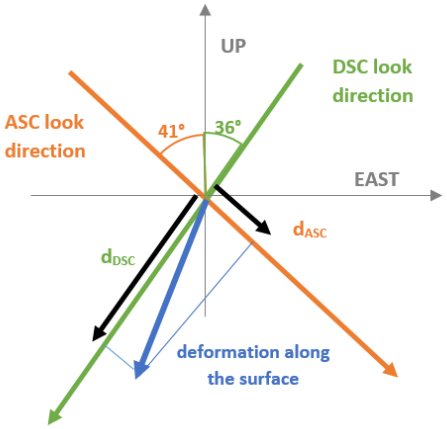

Reviewer 1, specific comment 9. Lines 261-264: The description of the two sides of the bowl is poorly supported by the figure.

Thanks for the comment, we added Fig. 3. based on source modelling to support the discussion.

Reviewer 1, specific comments 10. Lines 305-306: “guaranties to maintain coherence” – coherence is definitely not maintained in the central area.

We agree with the reviewer’s remark. It will be emphasized in the revised version of the ms. that the parameters of the Sentinel-1 mission, i.e. short revisit time, orbit positioning control, help to maintain coherence in general; however, any change in the surface backscatter properties can lead to coherence loss.

Reviewer 2, specific comment 1. The authors talked a lot about geological settings in Section 2 “Geographical and geological background”, but it looks not related to your discussions later in the paper. The same problem as in Section 3. Could you relate your deformation results to the geological settings and mining activities? Maybe you can add a section in discussion to talk about the relationship between deformation and geological setting/ mining activities.

We will add a section devoted to analytical modeling to explain the mechanism of sinkhole formation and its relation to mining activity in the area.

Reviewer 2, specific comment 5. I think your discussion is not enough, could you please talk about how the deformation results relate to the geological settings you described in Section 2.

We agree with the reviewer, the results of InSAR analysis is not coupled to the geological setting of the area, thank you for the comment. We will add a source modeling analysis, described above, to find a linkage between deformation evolution and geological setting and explain the subsurface processes.

Reviewer 1, technical corrections 1. The paper requires Language and grammar editing. Lots of sentences lack commas (,) to separate between parts of the sentence. Citation of previous studies should not be in brackets when they are the subject of the sentence. For example, line 143: (Gaidin, 2008) has already drew attention to: : :.., should be: Gaidin (2008) has already: : :.. This type of error appears many times in the paper. 2. Line 115: change horizontal extension to areal extent 3. Line 256: what is MT-InSAR? Fig. 7 is like 6 but descending

Reviewer 2, technical corrections: 1. Line 307, please check the citation format (Velasco et al.,
2017). And some of the same problems across the whole manuscript. 2. Line 221, Small Baseline Subset, SBAS -> Small Baseline Subset (SBAS) 3. Line 203, 1’ resolution SRTM, is it 1 arc second?

Thank you for your comments. We will thoroughly check the English of the ms.

Regarding citations: We used the Mendeley Citation plugin (https://www.mendeley.com/guides/using-citation-editor) for MS Word. It is a rather convenient tool for generating references, citations and bibliographies. We will check and adjust manually the citation format where necessary in the revised ms.

The 1’ resolution SRTM was released by USGS, we will add a proper reference in the revised ms, as:
Shuttle Radar Topography Mission 1 Arc-Second Global (Digital Object Identifier (DOI) number: /10.5066/F7PR7TFT

MT-InSAR stands for Multi-Temporal InSAR analysis, which is also called TS-InSAR (Time-Series InSAR) in the literature.

References

Agram, P. S., & Simons, M. (2015). Journal of Geophysical Research : Solid Earth A noise model for InSAR time series. *Journal of Geophysical Research : Solid Earth*, (May 2014), 1–20. https://doi.org/10.1002/2014JB011271.1.

Bagnardi, M., & Hooper, A. (2018). Inversion of Surface Deformation Data for Rapid Estimates of Source Parameters and Uncertainties: A Bayesian Approach. *Geochemistry, Geophysics, Geosystems*, *19*(7), 2194–2211. https://doi.org/10.1029/2018GC007585

Berardino, P., Fornaro, G., Lanari, R., & Sansosti, E. (2002). A new algorithm for surface deformation monitoring based on small baseline differential SAR interferograms. *IEEE Transactions on Geoscience and Remote Sensing*, *40*(11), 2375–2383. https://doi.org/10.1109/TGRS.2002.803792

Cao, Y., Li, Z., Wei, J., Hu, J., Duan, M., & Feng, G. (2018). Stochastic modeling for time series InSAR : with emphasis on atmospheric effects. *Journal of Geodesy*, *92*(2), 185–204. https://doi.org/10.1007/s00190-017-1055-5

Lisowski, M. (2007). Analytical volcano deformation source models. In *Volcano Deformation* (pp. 279–304). https://doi.org/10.1007/978-3-540-49302-0_8

Nof, R. N., Abelson, M., Raz, E., Magen, Y., Atzori, S., Salvi, S., & Baer, G. (2019). SAR Interferometry for Sinkhole Early Warning and Susceptibility Assessment along the Dead Sea, Israel. *Remote Sensing*, *11*(1), 89. https://doi.org/10.3390/rs11010089

Okada, Y. (1992). Internal deformation due to shear and tensile faults in a half-space. *Bulletin - Seismological Society of America*, *82*(2), 1018–1040.

Parizzi, A., Gonzalez, F. R., & Brcic, R. (2020). A covariance-based approach to merging InSAR and GNSS displacement rate measurements. *Remote Sensing*, *12*(2). https://doi.org/10.3390/rs12020300

Pascal, K., Neuberg, J., & Rivalta, E. (2013). On precisely modelling surface deformation due to interacting magma chambers and dykes. *Geophysical Journal International*, *196*(1), 253–278. https://doi.org/10.1093/gji/ggt343

SEGALL, P. (2010). *Earthquake and Volcano Deformation* (STU-Stud). Retrieved from http://www.jstor.org/stable/j.ctt7sg19

Wegmüller, U., Werner, C., Strozzi, T., Wiesmann, A., Frey, O., & Santoro, M. (2016). Sentinel-1 Support in the GAMMA Software. *Procedia Computer Science*, *100*, 1305–1312. https://doi.org/10.1016/j.procs.2016.09.246

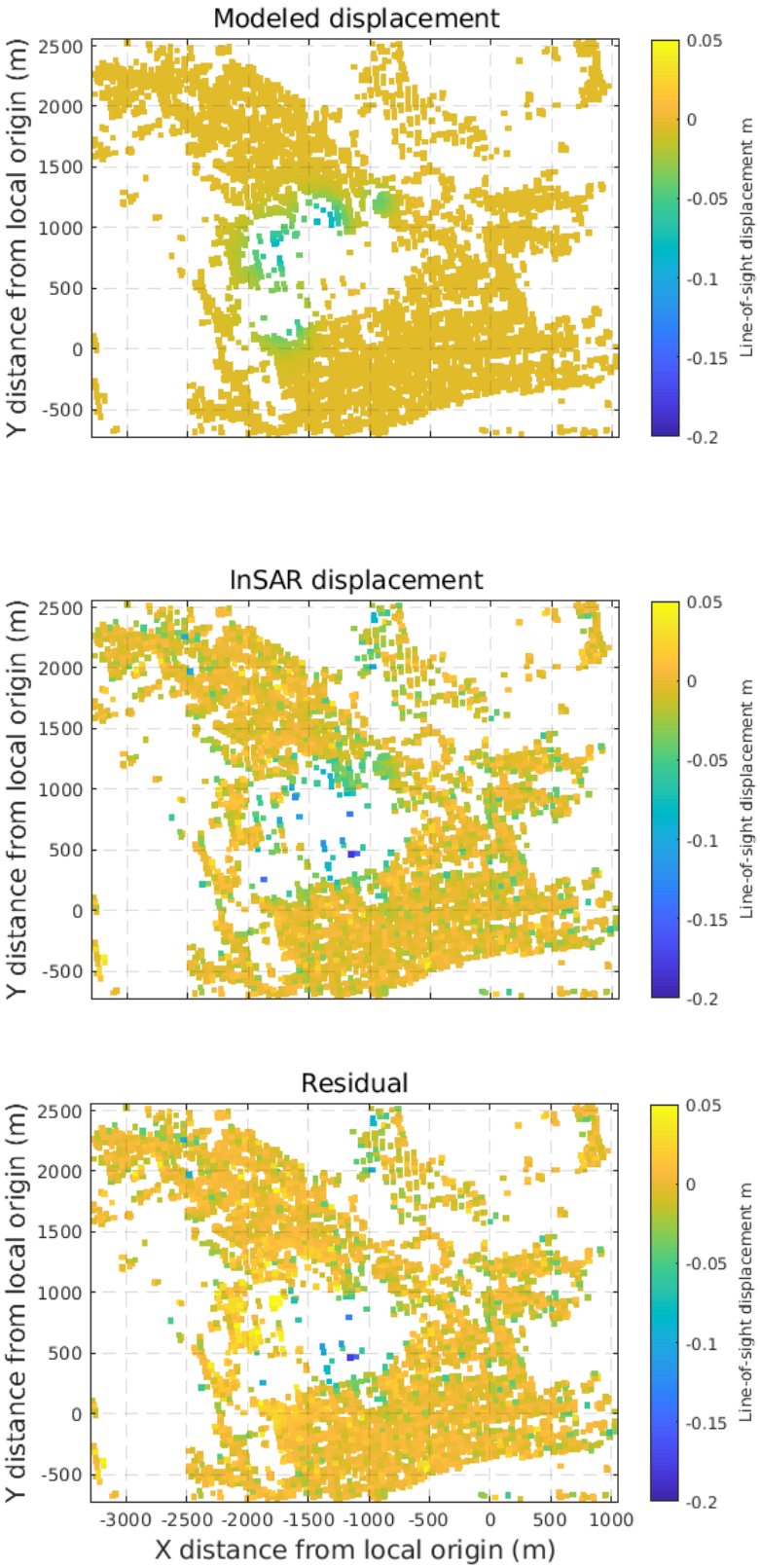

Fig. 1. Cumulative LoS deformation computed from the quad-configuration source model (top), deformation from the ascending Sentinel-1 observation (middle) and residuals after subtracting the best-fitting model

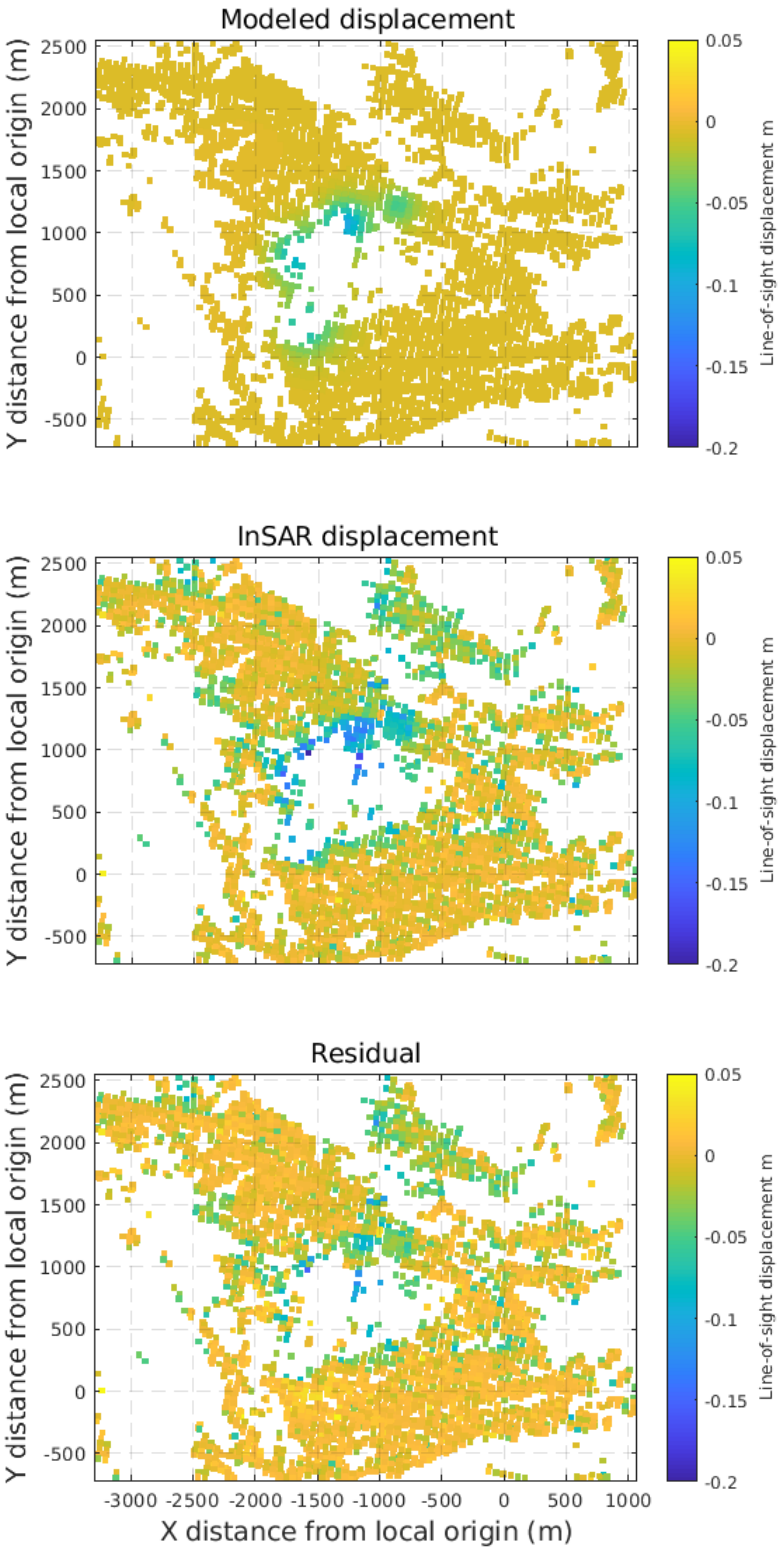

Fig. 2. Cumulative LoS deformation of the best-fitting model using four dislocation sources (top), deformation from the descending Sentinel-1 observation (middle) and residuals after subtracting the modeled displacement from the cumulative deformation

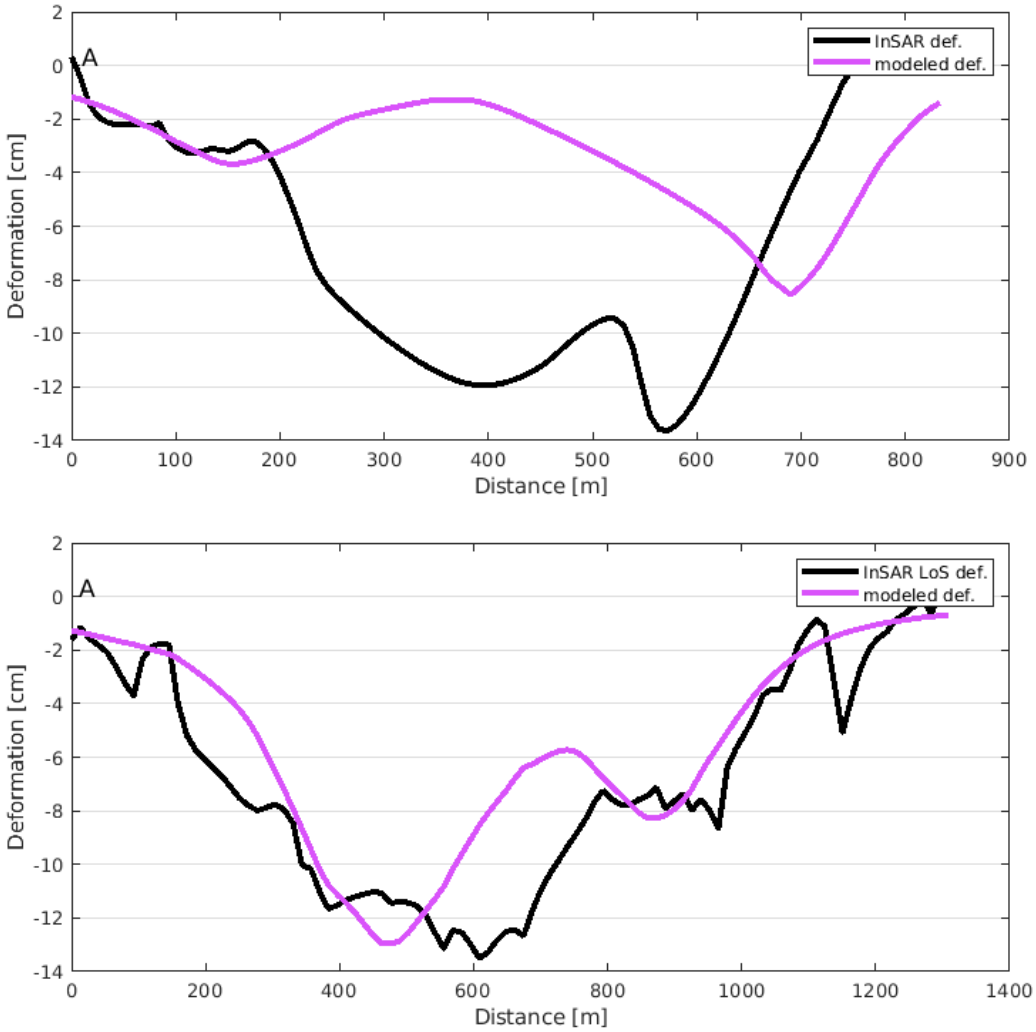

Fig. 3. Observed cumulative LoS and best-fitting model LoS deformations along selected profiles (given on Fig. 10. and 11. in the original ms.) for the ascending (top) and descending (bottom) passes.

Evolution of surface deformation related to salt extraction-caused sinkholes in Solotvyno (Ukraine) revealed by Sentinel-1 radar interferometry

Eszter Szűcs[1], Sándor Gönczy[2], István Bozsó[1], László Bányai[1], Alexandru Szakacs[3], Csilla Szárnya[1], Viktor Wesztergom[1]

[1] CSFK Geodetic and Geophysical Institute, Sopron, 9400, Hungary
[2] Department of Geography and Tourism, Ferenc Rakóczi II Transcarpathian Hungarian College of Higher Education, Berehove, Transcarpathia, Ukraine
[3] Institute of Geodynamics, Romanian Academy, Bucharest, Romania; Sapientia Hungarian University of Transylvania

Correspondence to: Eszter Szűcs (Szucs.Eszter@csfk.mta.hu)

Abstract. Rocksalt has remarkable mechanical properties and a high economic importance, however, ~~this~~ the strength of salt compared to other rocks, makes it a rather vulnerable material. Human activities could lead to acceleration of the dissolution of soluble rocksalt and collapse of subsurface caverns. Although sinkhole development can be considered a local geological disaster regarding the characteristic size of surface depressions the deformations can result in catastrophic events. In this study we report the spatiotemporal evolution of surface deformation in the Solotvyno salt mine area in Ukraine based on Sentinel-1 interferometric synthetic aperture radar measurements. Although the mining operations were finished in 2010 several sinkholes have been opened up since then. Our results show that ~~even though~~despite the enormous risk ~~managing~~ management efforts the sinkholes continue to expand with a maximum line-of-sight deformation rate of 5 cm/yr. The deformation time series show a rather linear feature and unfortunately no slowdown of the processes can be recognized based on the investigated 4.5 year-long data set. We utilized both ascending and descending satellite passes to discriminate the horizontal and vertical deformations and our results revealed that vertical deformation is much more ~~dominant~~ pronounced in the area. Analytical source modelling confirmed that the complex deformation pattern observed by Sentinel-1 radar interferometry has a direct connection to the former mining activity and is confined to the mining territory. With the 6-day repetition time of Sentinel-1 observations the evolution of surface changes can be detected in quasi real-time, which can facilitate disaster response and recovery.

keywords: Solotvyno salt mining, sinkholes, Sen~~t~~tinel-1 radar interferometry, surface deformation

1 Introduction

Large-volume rocksalt deposits formed in the Carpathian-Pannonian Region in its both internal (in the Transylvanian Basin) and external (along the outer margins of the Carpathian fold-and-thrust belt) parts during Badenian times, when those areas were communicating with each other. The Transylvanian Basin is a unique rocksalt storage, where salt layers of a few tens of meters thick were deposited, and later deformed by diapirism. Large volumes of salt migrated towards the margins of the basin due to the uneven loading of the overburden forming two basin margin-parallel belts of large-sized diapirs (Krézsek and Bally, 2006). ~~Less volumes were involved in smaller scale diapirism throughout the rest of the basin forming salt domes. The eastern diapir belt consists of much larger salt bodies (e.g the salt diapir at Praid is >2 000 m high) as compared to those in the western belt due to volcano basement interaction processes and increased heat flow along the nearby Călimani Gurghiu Harghita volcanic chain (Szakács & Krézsek, 2006).~~ Likewise, the salt layer deposited at the outer margin of the Carpathians, was deformed generating diapiric bodies known and exploited at many locations along the East Carpathians and South Carpathians in Ukraine and Romania. Solotvyno (Aknaszlatina, acc. to its local Hungarian name), located at the Ukrainian side of the northern East Carpathians, is one of them.

The western and eastern salt lineaments along the Transylvanian Basin, as well as the salt bodies along the external East- and South Carpathians offered a valuable mineral resource for centuries in the past. Salt is still extracted industrially at some of them. Nowadays, salt mines are again in the spotlight but for a different reason. Many of them, particularly the abandoned ones, pose a threat for populated residential areas, infrastructure and environment because the uncontrolled processes of suffusion and collapse of the old underground exploitation cavities (Deák et al.~~*et al.*~~, 2007~~,~~; Móga et al.~~ *et al.*~~, 2015, 2019~~, ;~~ Zechner~~ *et al.*~~et al., 2019). One of the severely affected localities is Solotvyno, where collapse of subsurface caverns in the past resulted in dolines, temporally filled with brine and have a size of 150-230 m in diameter. Fig. 1. illustrates the most recent deformation, which has started around 2012 and resulted in ~~shows some pictures of the existing sinkholes in the area, the~~the formation of twin sinkholes~~. shown on the left are the result the most recent deformations started in 2012.~~

~~[Please insert Fig. 1. near here]~~

Continuous monitoring of the evolution of such depressions and progression of sinkholes developed on top of old manmade excavations are essential to delineate unstable topographic surfaces and identify risk-prone areas in order to mitigate the threats. This requires high-resolution spatiotemporal observations (e.g. a dense network of measurement points) to follow and map the dynamics of the ongoing processes. Such a goal can be accomplished by using recently developed Earth observation techniques (Elliott et al., ~~, Walters and Wright,~~ 2016~~;~~, Li et al., 2016).

[Please insert Fig. 1. near here]

~~Interferometric synthetic aperture radar (InSAR) is a remote sensing technique which operates with microwaves. The satellite emits electromagnetic radiation and detects the reflected signal. By exploiting the coherent phase difference of the time-separated SAR scenes information on the possible ground deformation can be retrieved. ESA Copernicus Sentinel-1 mission is the first of its kind in the sense that it ensures coordinated global observations with unprecedentedly wide spatial coverage and with unrivaled measurement frequency (6 days for Europe and 12 days for other parts of the globe) and freely accessible for users (Sentinel-1 User Handbook). Therefore, Sentinel-1 radar interferometry enables to detect surface topographic changes from small-scale to high magnitude with a high density of measurements points, and due to the frequent repetition time of the satellite it allows to study the dynamics of numerous surface processes (Strozzi *et al.*, 2013; Elliott, Walters and Wright, 2016). The great advantage of the microwave radar interferometry is that it allows to monitor areas in all-weather conditions and to study surface deformations either of natural or anthropogenic origin even in areas with difficult access.~~

The objective of this study is to assess the current state of the salt mine-related deformations in the Solotvyno area caused by ground collapses in the past and to identify potential small-scale and dynamic surface variations related to dissolution cavities, which could result in further ground depressions and collapses of the abandoned salt-exploitation cavities in the future. Although the issue is well-known, no dedicated terrestrial monitoring network has been installed in the area yet. Therefore, Sentinel-1 satellite interferometry can be a unique opportunity to support the early identification of areas prone to sinkhole occurrence. The impact of salt dissolution related cavity collapse is not merely a local problem, but it could be amplified to a regional-scale issue in the future owing to the proximity of the Tisa river, one of the main rivers in Central-Eastern Europe crossing several borders (Ukraine, Slovakia, Hungary, Romania, Serbia). As the water infiltration caused sinkhole development propagates the boundary of the mining area, inhabited areas will be endangered. Some parts of the city have already been evacuated. However, besides the economic losses, the ecological impact of migrating brine into the underground freshwater system and eventually into the Tisa river can be catastrophic. Recognizing the environmental threat, the European Commission devoted considerable funds to support emergency preparedness, environmental protection, safety and security in the area. Pollution of the freshwater river with brine can have unforeseeable consequences similar to the environmental disaster caused by sequences of metal pollution originating from Romanian mining accidents at the beginning of 2000.

2 ~~Geographical and g~~Geological background and salt mining activities in Solotvyno

80% of the Ukrainian Subcarpathian territory is a mountainous area, the remaining 20% shows a low-lying flat topography including two parts: the Chop-Munkachevo plain and the Marmarosh ~~(~~or Solotvyno~~)~~ basin extending southward in Romania across the state border (Chis~~HIȘ~~ and Kosinszki~~OSINSZKI~~, 2011,~~;~~ Nakapelukh et al., 2017). The Solotvyno ~~area, hosting~~basin hosts most of the ~~a~~ shallow subsurface salt domes, 16~~, where the famous salt mines were excavated centuries ago, is part of this latter geomorphological unit . There are~~of ~~-~~19 in number, known ~~salt diapirs known~~ in the Ukrainian Subcarpathians

Subcarpathians, most of them (16) occurring in the Solotvyno basin (Bosevs'ka, 2015). Starting from the town of Khust in the west, this 50 km long and 22 km wide elongated basin extends with diminishing width in the ESE direction. Its Ukrainian part is bounded by the Vihorlat-Gutin Neogene volcanic range to the west and south, and the Carpathian thrust-and-fold belt to the north and east (Fig. 2).

[Please insert Fig. 2. near here]

The Solotvyno basin was initiated at the end of the Eggenburgian (Lower Miocene) when the fracture zones formed which determined the structural evolution of the whole Ukrainian Subcarpathian area (Fig. 3). These initial tectonic events generated a strongly segmented topographic surface. The tectonic activity in the area continued during Ottnangian times concurrently with the strong uplift of the Carpathian background area which resulted in the accumulation of the 20-60 m thick *Neogene basal conglomerates* in the marine and lagunal environment of the lowland areas. The sediment transport was oriented toward SW, in the direction of the shallow sea covering the Transylvanian Basin at that time (Tischler *et al.*, 2007; IŞTVAN, 2011). During the Carpathian period (Middle Miocene, Fig. 3a) rhyolite and dacite tuffs, as well as mudstone and marl sediments (composing the *Novoselytsa Formation*) were emplaced, with slight erosional unconformity, over the *Neogene Basal conglomerate* or, in places, over the rock complexes of the Paleogene basement. This formation represents the immediate basement of the salty deposits at Solovytno (Fig. 3) (Andreyeva-Grigorovich *et al.*, 1997; Gröger *et al.*, 2008; Wysocka *et al.*, 2016). In this time period the only marine sedimentary depocenter in the whole Ukrainian Subcarpathians existed in the central part of the Solovytno Basin. At the end of the Lower Carpathian period a ca. 300-400 m thick salt layer accumulated before the salt precipitating process ceased because the gradual invasion of freshwater from the neighboring Pannonian Basin and concurrent formation of terrigenous siliciclastic sequences.

At the beginning of the Badenian period (Fig. 3b) in the central part of the Subcarpathian Plain the *Tereblya Formation* (Fig. 4) composed dominantly by salt, less salty clay, sandstone, and minor amounts of gypsum and anhydrite was deposited in a bay with gradually diminishing salinity. This basin was connected to the open Paratethys sea probably across the Solovytno Basin and the Transylvanian Basin. It was surrounded by uplifted land areas with a still poorly developed hydrographic network. At the Lower Badenian–Upper Badenian boundary started the largest transgression event of the Miocene evolution of the Transcarpathian area (Fig. 2c) resulting in the deposition of the *Solotvyno Formation* (Fig. 4) composed mainly of sandstone, siltstone and claystone (Andreyeva-Grigorovich *et al.*, 1997; Ślączka *et al.*, 2007; Bukowski and Czapowski, 2009).

[Please insert Fig. 3. near here]

The Pannonian Basin and the smaller basins located behind the Carpathians were connected to each other across the Subcarpathian area of today. The Pannonian sea became significantly deeper having a higher than average salinity, however no (or very poor and localized) salt formation occurred because of the short time of increased salt concentration. Towards the end of middle Badenian times horst and graben structures formed in the Solotvyno Basin. The basin shallows down, laguna and delta facies sequences (the *Teresva Formation*) were deposited (Fig. 3. d.).

~~Near-shore laguna, delta and lacustrine-alluvial facies sediments are known at the Upper Badenian level. The tracks of the biggest rivers are found in the Tarac and Apsica valleys. Towards the end of the period indicators of lower salinity to brackish waters were identified in the deposited sedimentary sequences (*Baskhev Formation*) according to the change in the Foraminifera population, caused by the isolation from the Paratethis. In the northern part of the Solovytno Basin increasing proportions of lacustrine-alluvial sediments are present at this level. At the Badenian-Sarmatian boundary the Upper Badenian sea regression process is already completed. Sedimentary sequences formed during the new, Sarmatian transgression cycle are known along the western, eastern and southern peripheral bands of the basin, which were the only inundated territories. In the central and northern parts continental sediment-formation conditions prevailed. In places, low-energy sediment deposition processes dominate, whereas limited delta facies sediments are also present, and marsh environments were also identified. However, the sea present in this area at the beginning of the Sarmatian time was brackish with a ca.16-18 ‰ salinity.~~

~~[Please inser Fig. 4. near here]~~

~~3 Salt mining activities in Solotvyno~~

The Solotvyno salt diapir (Bosevs'ka and Khrushchov, 2011) has a remarkable size, with a horizontal extension of approximately 1 million m^2, ~~and~~ it has an elongated pear shape, oriented in the northwest - southeast direction (Fig. ~~5~~3. a and c). The largest ~~length~~ depth of the salt body is ca. 2 km, whereas its width varies between 200 and 800 m in the westernmost and easternmost parts, respectively. The salt diapir lies beneath a thick layer of gravel, embedded in sandstone at an average depth of 25-30 meters. The formation is covered with a thin, grey salt layer, the so-called pallag (layers of salt and clay) which functions as a waterproof layer, hindering the formation of natural salt karst. The earliest salt extractions were started by the method of dissolution, where the pallag layer was missing. As a result of the large-volume industrial mining, it was inevitable to cut through the sealing pallag layer which raised the possibility of flooding. Another factor, which makes the situation much more severe, is the c~~los~~loseness of the Tisa river. The river bed changed during time as the diapir emerged, and nowadays the river flows around the salt body from southern direction. The gradient of the river bed is ~~quite~~ rather high, about 15 m within a few kms (Fig. ~~5~~3. b.). During the great flood~~sing events~~ of the river the water infiltrates towards the salt body and causes serious damages, where the waterproof layers are missing. Such events happened in 1998, 2001 and 2007 (Móga et al., 2015, 2017) ~~and~~ contribut~~inged~~ to the shutdown of the mines.

Exploitation of salt in Solotvyno has a long history, however, the industrial-scale production only began in the 18th century. Since the starting of the first mine in 1778, a total of 10 mines were operating in the area ~~of Solotvyno~~ (Fig. ~~5~~3. ~~c~~d., Tabl. 1.). The 8th (Lajos) and the 9th mines were used for the longest time span, the others were operated for a relatively short period of time. At the end of the 1980s and beginning of 90s a new, so-called 10th mine was developed but there was no exploitation here at all (Bosevs'ka and Khrushchov, 2011). The available total salt reserves ~~available~~ are estimated at about 2 billion ~~tones~~tons. In the beginning of the 1990s about 10% of the Ukrainian salt production was mined in Solotvyno, with an estimated yearly rate of 500 ~~000~~ thousand ~~tones~~tons.

Prior to the industrial extraction of rocksalt, only small-scale karst formations were observed at the surface of the area affected by mining. The development of salt karst processes accelerated in such a way after the beginning of the large-volume industrial mining operations, that nowadays it is almost impossible to mine rocksalt at all.

[Please insert Fig. 3. near here]

~~[Please insert Fig. 5. near here]~~

[Please insert Tabl. 1. near here]

Environmental and economic problems of Solotvyno salt mines gained more and more public attention after 2000 and at the beginning of ~~in~~ 2010~~'s~~ the city was categorized by authorities as a disaster prone area.

Several studies were conducted in the past related to the salt operations, but these were limited to the investigation of the location, geology and formation conditions of the salt diapir and the possibilities of salt exploitation. ~~(~~Gaidin ~~(,~~ 2008) has already ~~drew~~ drawn attention to the problems of salt karst formation processes in 2008. He analyzed karst development thoroughly, presented the dissolution process of the pillars and the resulting stability change of mineshafts. ~~(~~Diakiv and Bilonizhka ~~(,~~ 2010) presented an overview of the geological outline of Solotvyno salt mine and in addition they described the ~~state~~ stage of salt karst formation in 2010 in detail. They also highlighted the poor conditions of the drainage system around the cultivated areas with an emphasis that it could lead to the leakage of an increased amount of freshwater into the karst system. ~~(~~Diakiv ~~(,~~ 2012) has also investigated the salt karst formation in the area based on the studies of two mines. ~~(~~Bosevs'ka and Khrushchov ~~(,~~ 2011) discussed the possibilities of disaster response and mitigation. Meanwhile, several research teams have simultaneously started to examine the ongoing surface processes and resulting formations mainly by ground-based geomorphological mapping procedures or participatory GIS analysis respectively (Móga et al., 2015, 2017~~,;~~ Onencan et al., ~~, Meesters and Van de Walle,~~ 2018).

~~3~~4 Material and methods

Interferometric synthetic aperture radar (InSAR) is a remote sensing technique which operates with microwaves. The satellite emits electromagnetic radiation and detects the ~~reflected~~ signal reflected from the surface. By exploiting the coherent phase difference of the time-separated SAR scenes information on the possible ground deformation can be retrieved. ~~ESA Copernicus Sentinel-1 mission is the first of its kind in the sense that it ensures coordinated global observations with unprecedentedly wide spatial coverage and with unrivaled measurement frequency (6 days for Europe and 12 days for other parts of the globe) and freely accessible for users (Sentinel-1 User Handbook). Therefore, Sentinel-1 radar interferometry enables to detect surface topographic changes from small-scale to high-magnitude with a high density of measurements points, and due to the frequent repetition time of the satellite it allows to study the dynamics of numerous surface processes (Elliott et al., 2016; Strozzi, Teatini, Tosi, Wegmüller, & Werner, 2013).~~ The great advantage of ~~the~~ microwave radar interferometry is that it allows to

monitor areas in all-weather conditions and to study surface deformations ~~either~~ of natural or anthropogenic origin even in areas with difficult access. The ESA Copernicus Sentinel-1 mission is the first of its kind in the sense that it ensures coordinated global observations with unprecedentedly wide spatial coverage and with unrivaled measurement frequency (6 days for Europe and 12 days for other parts of the globe) and freely accessible for users (Sentinel-1 User Handbook). Therefore, Sentinel-1 radar interferometry enables the detection of surface topographic changes from small-scale to high magnitude with a high density of measurements points, and due to the frequent repetition time of the satellite it allows to study the dynamics of numerous surface processes (Strozzi et al., 2013~~;~~, Elliott et al.~~, Walters and Wright~~, 2016).

~~Sinkholes can develop naturally in geological environment where soluble rocks like carbonate and evaporate occur. Human activity of underground mining or infrastructure development can influence the solubility of materials and increase the risk of subsurface cavern development (Dou *et al.*, 2015; Valenzuela *et al.*, 2015; La Rosa *et al.*, 2018; Scotto di Santolo, Forte and Santo, 2018; Nam and Shamet, 2020). Shallow mining activity can also be a source of sinkhole generation in locations where insufficient engineering measures to reduce surface deformation are performed, especially in post-mining territories (Perski *et al.*, 2009; Czikhardt *et al.*, 2017; Malinowska *et al.*, 2019). Several studies focus on the development of sinkhole susceptibility models e.g. (Galve *et al.*, 2008; Valenzuela *et al.*, 2015) taking into account factors as topography, geomorphology, geology, hydrological dynamics of the area, location of manmade structures to perform a GIS analysis and reveal the probability of sinkhole evolution. The applicability of such a comprehensive modelling heavily depends on the available data sets and their resolution. Therefore, various types of in-situ measurements are utilized to provide insight of the ongoing sinkhole related deformation processes. Detection of surface sagging, monitoring temporally and spatially of sinkhole evolution as well as detecting deformation after sinkhole remediation is essential nowadays specifically in urbanized environment to reduce the socio-economic impact of this kind of geohazard. A thorough review of sinkhole monitoring techniques with their advantages and limitations are discussed in the recent study by (Gutiérrez *et al.*, 2019). The size of the sinkhole prone area, the required resolution both in time and space of monitoring with its accuracy, the accessibility of the location, the land use and the required manpower all determine the approach or a combination of techniques to be utilized as (Gutiérrez *et al.*, 2019) demonstrated. Remote sensing techniques as radar interferometry offers a blanket cover of measurement points and high repetition time to detect surface deformation. InSAR (Bürgmann, Rosen, & Fielding, 2000; Simons & Rosen, 2007) proved to be a powerful and versatile tool to detect topographic changes as well as to perform historical analysis based on the availability plethora of archive and operational remote sensing data sets (ERS-1, 2, Envisat, PALSAR-1, 2, Sentinel-1 and commercial products).~~ Sentinel-1 is a twin constellation (Sentinel-1A was launched in 2014, B in 2016) of C-band (wavelength ~ 5.5 cm) satellites separated by 180° in~~ the~~ orbit. The main acquisition mode of Sentinel-1 over land is TOPS (Terrain Observation of Progressive Scans), which ~~implies~~ employs the generation of the wide swath, so-called IW mode (250 km) SAR products with medium spatial resolution (ca. 5 m x 20 m in range and azimuth directions, respectively). The narrow orbital tube of the satellites and the almost synchronized bursts of SAR scenes makes the IW products suitable for interferometric analysis.

43.1 Dataset

To assess the surface deformation caused by salt dissolution we used the available Sentinel-1 SAR collection covering the area of interest. The time period covered by Sentinel-1 is more than 4 years and it is sufficient to investigate the longer-term (i.ei.e. multi-annual) behavior of surface deformation processes and to detect possible new surface developments. Both ascending and descending data sets were utilized to facilitate the separation of total line-of-sight (LOSLOS) deformation into east-west and vertical components which can help to understand the mechanism of sinkhole collapse and the progress of underground processes. Details of the Sentinel-1 SAR dataset used in this study is summarized in Table 2. Significant change in surface scattering properties (e.g. snow cover) results in low quality interferograms, therefore winter scenes with snow cover were excluded from the analysis.

[Please insert Table 2 near here]

43.2 Multi-temporal, multi-baseline InSAR analysis

The characteristic scale of a sinkhole is about a few 10s of meters which can be considered as locally concentrated deformation in an InSAR analysis, affecting only a few pixels of a SAR scene compared to the broad spatial pattern of routinely investigated topographic variations (landslides, volcanic unrest, strain accumulation). In addition, sinkholes represent a quite unpredictable type of geohazard in the sense that the temporal evolution of salt dome caverns are mostly not observable at the surface directly, but high gradient surface deformations occurs suddenly, just before the failure (Jones and Blom, 2014). Therefore, the detection of such a small scale, almost episodic deformation can be challenging. Several studies demonstrated the potential of radar interferometry to characterize the post collapse deformation of sinkholes (Baer *et al.*, 2002; Galve, Castañeda and Gutiérrez, 2015; Kim *et al.*, 2016; Velasco *et al.*, 2017; La Rosa *et al.*, 2018) originating either from mining activity or triggered by seismic creep. There have been successful attempts to identify precursory deformations before the catastrophic collapse (Nof *et al.*, 2013; Jones and Blom, 2014; Malinowska *et al.*, 2019) .

The interferogram formation of Sentinel-1 IW SLC (Single Look Complex) images requires co-registration in azimuth direction of extreme accuracy due to the strong Doppler centroid variation within each burst (for more details see e.g. (Yague-Martinez et al., 2016;, Fattahi et al., Agram and Simons, 2017). For the precise co-registration of S1 scenes we followed the strategy described in (Wegmüuller et al.*et al.* (,2016). We applied S1 precise orbit ephemerides and the 1' resolution SRTM surface model (Reuter et al., Nelson and Jarvis, 2007, Shuttle Radar Topography Mission 1 Arc-Second Global Digital Object Identifier number: /10.5066/F7PR7TFT) to consider the effect of terrain topography during a matching procedure of SAR images, which the result of which werewas further refined using the Enhanced Spectral Diversity method (ESD) in the burst overlapping regions to reach a co-registration accuracy of an order of 1/1000 pixel. The ESD considers the double difference interferograms to determine the fine azimuth offset, therefore it is required to have coherent regions in the burst overlapping area. This requirement was met with several difficulties as the investigated area is sparsely populated and lacks of phase-stable

natural scatterers. Therefore, we applied a cascade co-registration strategy selecting a so-called ~~supermaster (reference)~~primary reference scene in the middle of the time series ~~in~~in the early spring period. Two ~~master~~ secondary reference scenes were selected for each year, one in spring when the vegetation hasn't started to thrive, and one in late autumn when only light vegetation covers the surface. These S1 scenes were co-registered directly to the ~~supermaster~~ primary reference scene and the rest of the scenes were co-registered to the primary reference ~~supermaster~~ using the nearest ~~master~~ secondary reference scene in time for ESD estimation. Based on the co-registered stack, the interferograms can be ~~determined~~ calculated in a standard way (Simons and Rosen, 2007).

Time series analysis of interferograms requires coherent scatterers with quite stable geometric and electromagnetic properties over time~~having geometric and electromagnetic properties quite stable over time~~. There are various techniques to select pixels, either dominated by a single scatterer or using averaged (multi-looked), noise-reduced distributed scatterers. These measurement points form the base of the time series analysis of differential interferograms either computed from a single-reference or a multi-reference stack (for more details on the comparison of different techniques see e.g. ~~(~~Crosetto et al. ~~(,~~ 2016~~);~~, Osmanoğlu et al. ~~(,~~ 2016), and~~;~~ Manunta et al.~~,~~ (2019). To capture the high deformation rate of sequential depression and to maximize the coherence offered by the short spatial baselines and high revisit time of Sentinel-1 mission, we used a multi-baseline approach of interferogram formation (usually called Small Baseline Subset ~~-~~ ~~,~~SBAS, ~~(~~Berardino et al.~~,~~ (2002)). The interferograms were generated using the Gamma software (Wegmüller et al., 2016). We considered pairs of four consecutive SAR scenes to include redundancy in the interferogram network, which facilitates reduction of errors. We utilized both phase-stable single scatterers (PS) as well as distributed targets (DS), which ensures long-term coherence. The initial set of PS candidates was selected based on the high temporal stability of the backscattering as well as the low spectral diversity. For the DS scatterers we used multilooking with a factor of 5 x 1 (5 samples in range and 1 in azimuth) to increase signal to noise ratio but keeping in mind the spatial extent of the sinkholes. Distributed targets resulted in a 15 m x 15 m pixel size in the slant range, which enables the detection of localized deformation caused by surface depression. The flat-earth phase and topographic phase were removed from the interferograms. In the multi-baseline approach interferograms were unwrapped in space first, finding the unambiguous phase values. The phase unwrapping was accomplished in an iterative way with quality control, keeping PS and DS pixels for the next step, which satisfy the phase model with reasonably small (< 1 rad) residuals. A two-dimensional phase model involving height corrections relative to the reference model (SRTM heights mapped to radar coordinates) and linear deformation rate was chosen. The residual phase consists of non-linear deformation phase, atmospheric propagation delay, error in the height correction estimates and other noise terms. The spatially correlated, low-frequency part of the residual phase was separated by spatial filtering from the residual phase, since unwrapping residual phase of point differential interferograms is much simpler than unwrapping the original point differential interferograms. The whole process was iterated starting from dividing the area into patches, where the linear phase model approximation was suitable. Using a multi-reference stack based on consecutive SAR scenes, the deformation phase can be kept as small as possible. With the constant refinement of the phase model, a single regression was applied on the whole area. The main output of the regression analysis was the unwrapped phase. The various phase terms were summed up and then the unwrapped phases were connected

in time and inverted to deformations using a least squares approach minimizing the sum of the square weighted residual phases (Berardino et al., 2002, Wegmüller et al., 2016). The atmospheric phase and non-uniform deformation phase are present in the time series of unwrapped phases. To discriminate between the two, we identified areas with high deformation rate and excluded those phase values to estimate atmospheric propagation delay. Atmospheric phases were determined as a combination of height dependent atmospheric delay plus the long-wavelength component of the SBAS inverted residual phase. We used a low-pass filter with a characteristic length of 5 km. Therefore, long-wavelength (> 5 km) non-linear deformation was mapped into atmospheric correction. However, the area affected by subsidence is rather localized, so we can assume no long-wavelength non-uniform deformation.

3.3 Decomposition of surface deformation

The ascending and descending satellite passes offer the possibility to resolve the observed ~~LOS~~LOS deformations to vertical and horizontal components (Hanssen, 2001; Pepe and Calò, 2017; Fuhrmann and Garthwaite, 2019). The viewing geometry of the LOS vector is defined by the ϑ incidence angle, measured between surface normal and look vector, and the α satellite heading~~Since the satellite passes pole to pole and illuminates the surface in right angle to the path the observed LOS deformation is the least sensitive to movements in the north-south direction.~~

$$d_{LOS} = [-\sin\vartheta\cos\alpha \quad \sin\vartheta\sin\alpha \quad \cos\vartheta]\begin{bmatrix} d_{EAST} \\ d_{NORTH} \\ d_{UP} \end{bmatrix}$$

Since the satellite passes pole-to-pole and illuminates the surface in right angle to the path, the observed LOS deformation is the least sensitive to movements in the north-south direction. –This component is usually neglected and the horizontal component of the movement is interpreted in terms of deformation only in the east-west direction. Based on the ϑ incidence angle of the reflecting point of the ground (Table 2.) the d_{UP} vertical and the d_{EAST} east-west component of the ~~movement~~deformation can be resolved (Fig. ~~12~~4):

$$\begin{bmatrix} d_{LOS}^{ASC} \\ d_{LOS}^{DSC} \end{bmatrix} = \begin{bmatrix} \sin\vartheta_1 & \cos\vartheta_1 \\ -\sin\vartheta_2 & \cos\vartheta_2 \end{bmatrix}\begin{bmatrix} d_{EAST} \\ d_{UP} \end{bmatrix}$$

[Please insert Fig. ~~12~~4. near here]

~~We considered pairs of four consecutive SAR scenes to include redundancy in the interferogram network which facilitates reduction of errors. We utilized both phase-stable single scatterers (PS) as well as distributed targets (DS) which ensures long-term coherence. For the latter we used multilooking with a factor of 5 x 1 (5 samples in range and 1 in azimuth) to increase signal to noise ratio but keeping in mind the spatial extent of the sinkholes. Distributed targets resulted in a 15 m x 15 m pixel size in the slant range which enables to detect localized deformation caused by surface depression. The flat-earth phase and topographic phase were removed from the interferograms. In the multi-baseline~~

~~approach interferograms were unwrapped in space first, finding the unambiguous phase values, then the unwrapped phases were connected in time and inverted to deformations using a least squares approach minimizing the sum of the square weighted residual phases (Berardino et al., 2002; Wegnüller et al., 2016).~~

~~5~~4 Results ~~and discussion~~

~~5~~4.1 ~~Multi-temporal InSAR analysis~~Observations

Time series analysis of Sentinel-1 interferograms reveals surface deformations beneath the city of Solotvyno and its surrounding. Based on the scattering properties of resolution elements a large number of pixels were identified (>35,000 on a ca. 9 km x 9 km area (supplementary Figs. 1, and 2) which densely cover the populated areas. Coherent points were also detected in the direct vicinity of the existing sinkholes in low-vegetation fields.

~~[Please insert Fig. 6. near here]~~

Fig. ~~6~~5. shows the linear ~~LOS~~LOS displacement rate determined from Sentinel-1 ascending data. The spatial pattern of the surface deformation computed from the ascending satellite pass data clearly shows the circular outline of the deforming area around the main sinkhole. Maximum deformation rate reaches almost 5 cm/yr (point 3 ~~i~~in Fig. ~~6~~5.) and located at the south-southeast part of the central sinkhole. The detected surface deformation forms patterns. Moderate, but persistent surface displacement with a magnitude up to 2 cm/yr is found north of the central sinkhole in an urbanized area (around point 1). Larger deformation rates occur south from the central sinkhole. Here, we identified two clusters of anomalous points, one patch located south-southeastwards from the central sinkhole with deformation rates varying between 4-5 cm/yr (around point 3). The other pattern is concentrated at the southwestern edge of the larger deforming area (point 2) with an average rate of 1-3 cm/yr. A localized deformation zone was found farther, ca. 2 km away, from the mining area in the west direction, on the left bank of the Tisza river. It's average rate is 1.2 cm/yr and it is located in the area with some small lakes (point 5).

[Please insert Fig. 5. near here]

The deformation rate is almost linear in the whole area, individual deformation time series for some selected points (mentioned in the text above) is given in Fig. ~~8~~7. No significant sudden movement was detected. The time evolution of the ~~LOS~~LOS surface deformation is shown in Fig. ~~10~~ 9. along a cross-section directed almost north-south (cross-section A-B). The path was selected to have the highest point density ~~in order to avoid spurious signals due to interpolation of scarce data points.~~ and a natural neighbor interpolation method was applied based on the points satisfying some distance criteria (< 50 m) around the location of the profile. Location of cross-sections was selected to get information in roughly perpendicular directions of the area, it was chosen by visual inspection of point distribution. Fig. ~~10~~ 9. nicely shows the different magnitudes of the deformation rate between the northern and southern parts of the area, as well as the highly linear characteristics of surface evolution.

[Please insert Fig. ~~7~~6. near here]

Regarding the descending Sentinel-1 interferogram time series ~~analysis~~, the average deformation rate shows a similar pattern compared to ~~as for~~ the ascending pass. This suggests that the deformation ~~consists~~ shows ~~mostly~~ primarily~~of~~ vertical ~~component~~behavior. Results from the MT-InSAR analysis ~~is~~ are shown in Fig. ~~7~~6. in terms of average linear deformation rate. The movement north from the central sinkhole is much more pronounced and affects an extended area (see point 5). Deformation possibly related to landslide activity is captured on the hillside in the upper northern part of the figure, which was previously identified by ~~(~~Velasco et al. ~~(,~~2017). This movement along the gradient of the slope was not pronounced in the ascending satellite geometry. The growth of the disturbed area in time is illustrated in Fig. ~~11~~10. on an east-west cross~~-~~section (marked by C-D) in the northern part of the investigated area. The motion is very linear in time, but shows an asymmetric shape in the east- west direction. The western part of the cross-section (the distance from point ~~A~~ C is about 600 m) is ~~resembles~~ much more similar to a classical subsidence bowl, whereas the eastern side (between 600 m and 1200 m) shows a sharp step (section from 600 m to 800 m). This part of the area, which moves like a solid block, is covered with buildings. Fig. ~~9~~8. shows the individual time series of the points marked in Fig ~~7~~6.

[Please insert Figs. ~~8~~7. and ~~9~~8. near here]

[Please insert Figs. ~~10~~9. and 10~~1~~. near here]

~~5~~4.2 Decomposition of surface deformation

The different acquisition geometry results in dissimilar measurement points for the ascending and descending passes. To overcome this limitation and combine deformation rate results from ascending and descending passes, the data sets are usually interpolated to a common grid resulting in so-called pseudo measurement points (Ferretti, 2014). Besides the common spatial grid, a common zero reference point is required to make datasets obtained from different acquisition geometries comparable. In our study both data sets were referred to the same reference point, which is located far enough from the deforming area in the east direction (marked with white cross in the supplementary Figs). As the time series analysis revealed that the surface deformation is quite linear, we combined the deformation rates and not the deformations directly. Results of LOS decomposition are given in Figs. 11. and 12. for the vertical and east-west (positive towards east) directions, respectively. Interpretation of vertical and horizontal deformations are more straightforward than explanation of LOS displacements and gives a coarse estimate on the ongoing processes. As Fig. 11. and 12 show, vertical deformation is more pronounced in the area, the vertical velocities are about twice in magnitude compared to the horizontal velocities. Although the most recent cavity collapse related to the abandoned mines occurred around 2012 in the northern (9th mine) and in the southern (8th mine with the twin dolinas) parts of the area subsidence is still in progress. The highest rates, ranging from 2.5-4.5 cm/yr, are recorded in the inner zone of the central sinkhole, whereas at the northern and southern edges of the deforming area deformation is still remarkable with a magnitude of 0.5 – 1.5 cm/yr. Regarding deformations in the east-west direction (Fig. 12.), the magnitude of the displacement is much smaller, the maximum rate being about 2 cm/yr. The complex surficial depression pattern suggests

that the subsidence presumably originates from several individual sources or from the superposition of subsurface caverns. The northern part of the deforming area clearly shows a westward displacement, whereas its southern part shows displacement towards the east. The lack of InSAR observations impedes the retrieval the whole deformation signal, i.e. the alternating east-west pattern generated by a single subsidence void, therefore it can be only concluded that the deforming area is still actively growing nowadays.

[Please insert Figs. 11. & 12. here]

~~The ascending and descending satellite passes offer the possibility to resolve the observed LOS deformations to vertical and horizontal components (Fuhrmann & Garthwaite, 2019; Hanssen, 2001; Pepe & Calò, 2017). Since the satellite passes pole-to-pole and illuminates the surface in right angle to the path the observed LOS deformation is the least sensitive to movements in the north-south direction. This component is usually neglected and the horizontal component of the movement is interpreted in terms of deformation only in the east-west direction. Based on the ϑ incidence angle of the reflecting point of the ground (Table 2.) the d_{UP} vertical and the d_{EAST} east-west component of the movement can be resolved (Fig. 12):~~

$$\begin{bmatrix} d_{LOS}^{ASC} \\ d_{LOS}^{DSC} \end{bmatrix} = \begin{bmatrix} \sin\vartheta_1 & \cos\vartheta_1 \\ -\sin\vartheta_2 & \cos\vartheta_2 \end{bmatrix} \begin{bmatrix} d_{EAST} \\ d_{UP} \end{bmatrix}$$

~~[Please insert Fig. 12. near here]~~

~~The different acquisition geometry results in dissimilar measurement points for the ascending and descending passes. To overcome this limitation and combine deformation rate results from ascending and descending passes the data sets are usually interpolated to a common grid resulting in so-called pseudo measurement points (Ferretti, 2014). Besides the common spatial grid, a common zero reference point is required to make datasets obtained from different acquisition geometries comparable. In our study both data sets were referred to the same reference point, which is located far enough from the deforming area in the east direction (marked with white cross in the supplementary Figs). As the time-series analysis revealed that the surface deformation is quite linear, we combined the deformation rates and not the deformations directly. Results of LOS decomposition is given in Figs. 13. and 14. for the vertical and east-west (positive towards east) directions, respectively. As Fig. 13. shows vertical deformation is dominant in the area: more than 80 % of the ongoing deformation is due to subsidence as compared to the total deformation. Although the most recent cavity collapse related to the abandoned mines occurred around 2012 in the northern (No. 9 mine) and in the southern (Lajos mine with the twin dolinas) parts of the area subsidence still in progress. The highest rates, ranging from 2.5–4.5 cm/yr, are recorded in the inner zone of the central sinkhole, whereas at the northern and southern edges of the deforming area deformation is still remarkable with a magnitude of 0.5 – 1.5 cm/yr. Regarding deformations in the east-west direction (Fig. 14.), the magnitude of the displacement is much smaller, the maximum rate being about 2 cm/yr. However, the pattern of the horizontal movement is still remarkable. The northern part of the deforming area clearly shows a westward displacement, whereas its southern part shows displacement towards the east. This pattern supports the concept that the deforming area is still actively growing nowadays.~~

~~[Please insert Figs. 13. & 4. here]~~

~~5~~4.3 Comparison with previous results

~~As mentioned in Section 5.1 a~~A previous study conducted by TRE Altamira (Velasco et al., 2017) investigated the potential of radar interferometry to monitor surface deformations caused by mining operations in the Solotvyno area in a framework of a contract with the Hungarian National Directorate General for Disaster Management. An exhaustive study was conducted based on archive C-band SAR datasets as ERS (1997-2001), Envisat (2002-2010) and Sentinel-1 (2014-2016) as well as high resolution X-band Cosmo-SkyMed (2016-2017, 4 months) acquisitions utilizing the SqueeSAR algorithm (Ferretti, 2014) which combines high resolution PS points with coherent DS scatterers. Although the study covers almost 20 years, the number of images used from former missions is quite low, for archive data set: 29 (ERS) and 30 (Envisat) imagesines were used compared to the contemporary Sentinel-1 mission with 44 SAR scenes. Archive data covers the investigated time period unevenly, therefore the resolution of the deformation time series may be inadequate which inherently raises the question of ~~aliasing of the~~ potential signal aliasing. The large collection of data from ESA's Sentinel-1 mission with frequent acquisitions guarantees ~~guaranties~~ to maintain the coherence in general and fosters the analysis of ~~to detect~~ the dynamics of surface deformation.

Using the C-band satellites, ~~(~~Velasco et al.~~,~~ (2017) could not really identify phase stable points in the direct vicinity of the sinkholes. Deformation rates (maximum 25 mm/yr away from the satellite, on average) occur~~s~~ in north and south directions from the main sinkhole mostly in urbanized areas. The three C-band results are very consistent with each other both in magnitude and pattern. Investigations based on the Cosmo-SkyMed data identified much more measurement points and gave almost uniform point distribution for the whole area. Several locations were detected in the inner zone around the main sinkhole with a cumulated magnitude of deformation as high as 40 mm for 4 months, which is equivalent to more than 10 cm/yr average deformation rate assuming a constant characteristic. It is quite interesting, however, that the pronounced deformation pattern located north-east of the main sinkhole in an industrial area, detected in all C-band datasets, was not identified at all. Although it should have an average value around 5-7 mm/yr, taking into consideration the short timespan of the investigated ~~short time span~~dataset, no measurement points were identified in the area of question. The study by ~~(~~Velasco et al.~~,~~ (2017) utilized satellite data only for descending pass compared to our investigations. For a meaningful comparison of the two studies we focused only on the datasets from C-band satellites. ~~(~~Velasco et al. (~~,~~2017) concluded that there was a lack of coherent scatterers over the area around the sinkhole and deformation rate could be detected for inhabited areas only. These surface changes concentrated mostly to the north of the deforming area, also identified in this study, but we detected measurement points in thinly vegetated areas too. The longer time span of this study confirmed that in the area of interest deformation is still ongoing. For the displacement history curves (Figs. ~~9~~ 7. and ~~10~~8.) it can be concluded that uniform deformation model is adequate to interpret the results, no acceleration or slowing down trend can be identified.

5. Source modeling

We modeled the deformation observed by InSAR in order to better understand the mechanisms responsible for the sinkhole growth, and constrain the location and depth of underground cavities which can result in sinkhole collapse in the future. The cavity deflation was modeled using rectangular dislocation sources (Okada, 1992, Segall, 2010) within a homogeneous and isotropic elastic half-space. We used a rectangular pressurized crack model, since deformations are presumably related to the destruction of abandoned mines. Despite their simplicity and the inherited approximations, analytical formulations are convenient to model and explain deformation patterns described by a few model parameters. The elasticity assumption implies that the half-space obeys Hooke's law, therefore displacements are considered infinitely small compared to the characteristic size of source dimensions (Lisowski, 2007). The observed gradual subsidence also supports the assumption of pure elastic deformation.

Unfortunately, no reliable information is available on the exact position, extension, orientation and depth of the mining underground. The estimated depth of underground mines varies between 50 m to 400 m, from the center to the perimeter of the mining area. The approximate location of the mines was estimated based on the available maps. We fit simple Okada rectangular dislocation models to the InSAR data using a grid-search method to estimate the initial model parameters. These were refined in a second step based on a Bayesian inversion.

5.1 Forward modeling

The coarse estimation of model parameters was accomplished by forward modeling varying source model parameters on a predefined interval. The parameter space of the dislocation models was constrained based on the rough location, geometry and orientation of underground mines available on maps as well as the approximate depth of the salt layer. Lack of coherence, either due to change in ground cover or high rate of deformation, does not allow to retrieve the entire deformation pattern associated with sinkhole evolution. Therefore, cumulative deformations from ascending and descending satellite passes covering the same time period were utilized simultaneously to increase the reliability of source model parameter estimation. The lack of deformation signal around the center of the area of interest makes it difficult to identify the number of source models required to explain the subsidence pattern. We made an exhaustive search for the best-fitting models using the misfit function

$$\delta = \left[\sum_{i=1}^{N}\sum_{j=1}^{M}\left(d_i - d_{i,m_j}\right)^2 / N\right]^{1/2},$$

where *N* is the total number of measurement points, *M* is the number of source models, d_i is the observed cumulative surface deformation and d_{i,m_j} is the modeled deformation from the jth source model projected onto the satellite LOS. Our results suggest a quad-source configuration of subsurface cavities; the model parameters are provided in Tabl. 3.

5.2 Source parameter estimation based on Bayesian inversion

To refine the source parameters and estimate associated uncertainties we performed a Bayesian probabilistic inversion (Bagnardi and Hooper, 2018). We modified the open-source GBIS (Geodetic Bayesian Inversion Software, http://comet.nerc.ac.uk/gbis/) code to handle custom source models of multiple rectangular dislocations. We also jointly inverted the cumulative ascending and descending InSAR data to determine deformation source parameters, i.e. horizontal dimensions and horizontal coordinates of rectangular source, depth of dislocation, strike angle of horizontal edge with respect to the north and opening of model (related to volume change), for every model in a single run. Within a Bayesian inversion approach the characterization of posterior probability density functions (PDFs) of source model parameters are accomplished by taking into account uncertainties in the data. The optimal set of source parameters can be extracted from the posterior PDF by finding the maximum a posteriori probability solution. The PDFs of source model parameters are determined from the likelihood function of the residuals between the observations and the model prediction weighted with the inverse of the variance-covariance matrix of the observations. The Bayesian inversion approach requires the quantification of errors in the data, which are assumed to be multivariate Gaussian with zero mean and covariance matrix. For multiple independent data sets, the likelihood function can be formulated as the product of the likelihoods of the individual data sets. To increase the numerical efficiency, the GBIS inversion algorithm samples the posterior PDFs through a Markov chain Monte Carlo method, incorporating the Metropolis-Hastings algorithm, with automatic step size selection. For more details, we refer to Bagnardi and Hooper (2018).

Noise covariance of individual interferograms has been well studied, the main error sources are the noise caused by the temporally correlated phase decorrelation and the spatially correlated atmospheric phase delay. Since InSAR observations are inherently relative, the additive phase delays make the accuracy of measurements strongly dependent on the distance. There have been several endeavors to provide an error analysis of time series InSAR output (see e.g. Agram and Simons, 2015; Cao et al., 2018 and references therein), however, we followed the method of Parizzi et al. (2020) and estimated the variance-covariance matrix of InSAR data sets experimentally. As Parizzi et al. (2020) points out, short time separated interferograms (supported by Sentinel-1 mission with multi-baseline analysis) are much more dominated by atmospheric propagation delay rather than phase variation due to deformation. After atmospheric phase correction the interferometric measurement error is practically the residual atmospheric phase delay, as short time separated interferograms can be considered deformation-free. The mean variograms of the residual atmospheric phase shows a stationary behavior and can be approximated by a covariance function. Since both deformation and average velocity are related to the phase by a scale factor, the error estimates can be simply computed. We used an exponential covariance model fitted to the data to determine the variance-covariance matrix of deformation in the Bayesian inversion. For both the ascending and descending data sets similar models were obtained with a moderate range values of 2.4 and 2.2 km for the ascending and descending datasets respectively.

Best-fit model parameters obtained from the forward modeling were utilized as starting values for the Bayesian parameter estimation. During the inversion the parameters were allowed to vary within reasonable limits taking into account the

geological constraints and information of past mining activity. The optimal model parameters are summarized in Tabl. 3., coordinates are given in a local rectangular coordinate system. Our final model assumes four rectangular-shaped subsurface cavities, developed in the salt layer. One source with a rectangular dislocation (model #1) of size 24.1 m × 64 m is located above the eastern edge of working panels of mine 9th at an estimated depth of 199.7 m. This mine was closed in 2008 due to water inrush. The moderate value of volume change suggests that this depression is an early stage of sinkhole development. The second source model (model #2) lies approximately 400 m southwest far from the first one and has a horizontal dimension of 63.5 m × 187.8 m, the required height change explaining the deformation pattern is -1.2 m. The elongated shape in roughly north-south direction of the source model is in agreement with the subsurface mining activity. Between the main corridors of mines 9th and 10th, long working panels were cut with varying length between a few tens to a few hundreds of meters. The third dislocation model (model #3) is located in the western periphery of the area affected by deformations. The model is roughly symmetric with a horizontal side length about 80 m and located at a depth of 273.1 m. There are several shallow mines there (numbered by 1 to 5 on Fig. 3. d.), established around the 18-19th century. These were completely destroyed as the numerous, small-scale dolines filled with brine indicate on the surface. The source model parameters suggest that the inverse modeling tried to find a global solution for the observed subsidence pattern. However, a single source is unable to sufficiently explain the complex deformation pattern; a number of near-surface, small-scale voids, related to salt dissolution are needed as well. The fourth source model (model #4) is located beneath the working panels of mine 8th, where heavy subsidence occurred around 2010, which resulted in the formation of the twin lakes. The depth of the model is about 296 m, the horizontal extension of the model is 72.3 m × 82.1 m. The estimated opening equals to approximately an 18,000 m^3 volume change. Taking into account the horizontal extension of the existing surface depressions of the nearby twin lakes, 15,000 and 17,000 m^2 respectively, our modeling results seem reasonable. The question, whether a new doline will form and will merge with the existing two in the future whether the boundary of the area affected by subsidence will expand toward the south, requires further observations with other tools besides radar interferometry.

Regarding the quantitative analysis of the inversion results Figs. 13. and 14. show the LOS deformation determined from the best-fitting quad-configuration source model (top), the Sentinel-1 cumulative LOS deformations (middle) as well as the difference between the observed and modeled values (bottom), for both the ascending and descending passes respectively. It can be assessed that the main features of the subsidence pattern on the northern and southern periphery are reasonably well captured by the source models. However, the modeled deformation on the western part of the area does not fit the observations, especially when compared to the ascending data set, where modeled deformation overestimates the observed ones. As it was mentioned, under this area the salt layer upwells close to the surface and many small dropout dolines have already formed and a single source model cannot adequately explain the surface deformation pattern.

Apart from larger discrepancies at some individual points the modeled deformation pattern fits well to the observed ones. However, one has to keep in mind when evaluating the inversion performance, that it was not possible to properly sample the deformation pattern with InSAR, as only the margins of the area were mapped adequately. Due to the sparse InSAR observation

distribution in the middle of the area, we could not fit a proper source model there, which can be seen immediately when inspecting the modeled and observed deformations along selected profiles given on Fig. 15. (same profiles as cross-sections A-B and C-D). Regarding the ascending data set, the same north-south oriented profile was used to check the model fit to InSAR observations as shown Fig. 9. to check the subsidence evolution in time. In the northern part (starting from point A to appr. 200 m) of the cross-section the source models are capable to explain reasonably well the observed deformation. The misfit of the modeled deformation is characterized by a standard deviation (std.) of ± 0.49 cm. However, for the second half of the investigated profile, between 200 and 800 m, the modeled deformation differs significantly from the observed ones. The reason for the large discrepancies in the middle of the cross-section comes from the fact, that it was not possible to find a proper source model based on the very scarce InSAR observations in the center of the area. On the southern edge of the cross-section (between 700 and 800 m) the applied single source model is not capable of resolving the observed deformation. Probably the InSAR derived deformations reflect the effect of more than one subsurface cavern. Fig. 15. b. shows the observed and modelled deformations in a roughly east-west cross-section (C-D, for the location please check Fig. 10.). Modeled deformation shows a reasonably sufficient fit to the InSAR deformations. The misfit of the model is characterized by a ± 1.87 cm std. The magnitude of the observed deformation is adequately described by the model, however, the location of extremities is slightly miss-estimated. The profile crosses the area in the north, where model #1 and model #2 is located. The effect of the two source models can be separated on the modeled deformations. Of course, the fine details revealed by InSAR observations cannot be reproduced by analytical modeling. Despite the simple formulas, analytical models can produce reasonable first-order results of the subsurface processes. Besides the above limitations it should be mentioned, that the possible interaction between the sources were not considered during the computation. As Pascal et al. (2013) pointed out, superposition of analytical models requires attention for adjacent models.

6 Discussion

Although the detection of small-scale, episodic deformation related to sinkhole generation can be challenging, several studies demonstrated the potential of radar interferometry to characterize the post-collapse deformation of sinkholes (Baer et al., 2002, Galve et al., 2015, Kim et al., 2016, La Rosa et al., 2018), and there have been successful attempts to identify precursory deformations before the catastrophic collapse (Nof et al., 2013, Jones and Blom, 2014, Malinowska et al., 2019). In this study Sentinel-1 radar interferometry was utilized to investigate surface evolution in a salt karst environment, where land cover differs significantly from area to area, where sinkhole detection can be monitored almost semi-automatically. Several factors such as, the complex geological conditions (relatively large and shallow salt structure), the specific hydrological setting (wet and warm continental climate with increased precipitation rate in warm season, close proximity of a main river) and the mining conditions (damaged waterproof layer, mining levels at different depth, cracks in the rock masses) increase the susceptibility of sinkhole evolution. In this regard a single case study cannot serve to draw general conclusions on sinkhole generation

mechanism, however, the experiences can be invaluable for making assessments and optimizing future monitoring methodology.

The Sentinel-1 radar interferometry results show that the detection of sinkhole evolution is feasible in the area, although it should be remarked that the point density of PS and DS scatterers is not sufficiently homogeneous. The complexity of the mechanism driving surface deformation as well as the inadequate sampling of the deformation pattern was revealed while explaining the subsidence pattern above the mining area by utilizing analytical modelling. Despite the limitations of the analytical formulas the assumed elastic rheology fits well to the temporal behaviour of surface deformation, which implies that the cavity evolution is in its early stage. The gradual surface subsidence suggested by the elastic deformation also agrees with the geological conditions of the area. Geomorphological investigations (Móga et. al, 2015) confirmed that the main driving mechanism of sinkhole formation in the area is much more like the mechanism of the perfect suffosion of non-cohesive soils, than the sudden dropout of cohesive soils. The spatial distribution of observed surface deformations advocates that the subsidence is confined to the territory of the mining area, which implies that natural salt karst processes are initiated and accelerated by the anthropogenic intervention. As no deceleration of the ground movement was observed, it suggests that the dissolution of subsurface salt layers has become a self-sustaining geological process.

7 ~~6 C~~Conclusions

Salt mining operations in Solotvyno obviously demonstrate the severe and long-term consequences of a reckless industrial salt exploitation. In a sense, the mining area now has become a natural laboratory, where salt karst processes evolving much faster than in carbonate rock can be studied in great detail. Based on Sentinel-1 SAR interferometry we have demonstrated that significant surface deformation is still ongoing nowadays related to the former salt mining operations. We revealed a cumulative line-of-sight deformation up to nearly 15 cm in 4.5 years. It was also shown that the deformation has a pronounced linear trend which suggests further steps to be done by local authorities in order to stabilize the mineshafts and improve the drainage system. Although several sinkholes have been opened in the last 20 years the geomorphological processes haven't ended yet, but there are hundreds of meters of intact mining holes that could pose a natural geohazard risk in the future.

Acknowledgement

Sentinel-1 data are copyrighted by the European Space Agency, and are additionally distributed by the Alaska Satellite Facility.

Author Contributions: Conceptualization E. Sz., V. W.; methodology and SAR data analysis I. B., L. B., Cs. Sz.; geological and geographical background S. G., A. S., interpretation E. Sz., V. W.. ~~, w~~Writing the original draft ~~ALL.~~and making corrections during the review process: ALL.

Funding: E.Sz, I. B., L. B. and Cs. Sz. wereas supported by the National Excellence Program grant No. 2018-1.2.1-NKP-2018-00007.

Conflicts of Interest: The authors declare no conflict of interest.

References

Agram, P. S., Simons, M.: A noise model for InSAR time series. Journal of Geophysical Research: Solid Earth, 120(4), 2752–2771. https://doi.org/10.1002/2014JB011271, 2015

Baer, G., Schattner, U., Wachs, D., Sandwell, D., Wdowinski, S., Frydman, S. (2002). The lowest place on Earth is subsiding—An InSAR (interferometric synthetic aperture radar) perspective. GSA Bulletin, 114 (1): 12–23. doi: https://doi.org/10.1130/0016-7606(2002)114<0012:TLPOEI>2.0.CO;2, 2002

Baer, G. *et al.* (2002) 'The lowest place on Earth is subsiding—An InSAR (interferometric synthetic aperture radar) perspective', *Geological Society of America Bulletin*, 114(1), pp. 12–23. doi: 10.1130/0016-7606(2002)114<0012:TLPOEI>2.0.CO;2.

Bagnardi, M., Hooper, A.: Inversion of Surface Deformation Data for Rapid Estimates of Source Parameters and Uncertainties: A Bayesian Approach. Geochemistry, Geophysics, Geosystems, 19(7), 2194–2211. https://doi.org/10.1029/2018GC007585, 2018

Berardino, P., Fornaro, G., Lanari, R., Sansosti, E.: A new algorithm for surface deformation monitoring based on small baseline differential SAR interferograms. IEEE Transactions on Geoscience and Remote Sensing, 40(11), 2375–2383. https://doi.org/10.1109/TGRS.2002.803792, 2002

Berardino, P. *et al.* (2002) 'A new algorithm for surface deformation monitoring based on small baseline differential SAR interferograms', *IEEE Transactions on Geoscience and Remote Sensing*, 40(11), pp. 2375–2383. doi: 10.1109/TGRS.2002.803792.

Bosevs'ka, L.: (2015) 'Structural and lithological characteristics Salt diapir Transcarpatia', Journal of Geology, Geography and Geoecology, 21(3/2). doi: https://doi.org/10.15421/111307, 2015

.

Bosevs'ka, L., and Khrushchov, D.: Environmental emergency in Solotvino: causes and geological problems solution strategy, (2011) 'ENVIRONMENTA EMERGENCY IN SOLOTVINO: CAUSES AND GEOLOGICAL PROBLEMS

SOLUTION STRATEGY', Journal of Geology, Geography and Geoecology, 19(3/2 SE-). doi: https://doi.org/10.15421/111117, 2011

Cao, Y., Li, Z., Wei, J., Hu, J., Duan, M., Feng, G.: Stochastic modeling for time series InSAR : with emphasis on atmospheric effects. Journal of Geodesy, 92(2), 185–204. https://doi.org/10.1007/s00190-017-1055-5, 2018

.

Chis, V. T., Kosinszki, S.: Geographical introductary characterization of the upper Tisa River basin (Romania-Ukraine), Transylv. Rev. Syst. Ecol. Res., 11, 1–14., 2011

Cis P.M. 1962: The geomorphology of USSR. – Publishing house of Lviv University. 244. (In Ukrainian)

CHIȘ, V. T. and KOSINSZKI, S. (2011) 'GEOGRAPHICAL INTRODUCTARY CHARACTERIZATION OF THE UPPER TISA RIVER BASIN (ROMANIA-UKRAINE)', *Transylv. Rev. Syst. Ecol. Res.*, 11(The Upper Tisa River Basin), pp. 1–14.

Crosetto, M., Monserrat, O., Cuevas-González, M., Devanthéry, N., Crippa, B.: Persistent Scatterer Interferometry: A review, ISPRS Journal of Photogrammetry and Remote Sensing, 115, 78–89. https://doi.org/10.1016/j.isprsjprs.2015.10.011, 2016

Crosetto, M. *et al.* (2016) 'Persistent Scatterer Interferometry: A review', *ISPRS Journal of Photogrammetry and Remote Sensing*. International Society for Photogrammetry and Remote Sensing, Inc. (ISPRS), 115, pp. 78–89. doi: 10.1016/j.isprsjprs.2015.10.011.

Deák, G., Mihai, S., Deák, Ș. E., Oancea, I.: Addressing the risk of surface water intrusion in old Romanian salt mines. Mine Water and the Environment, 26(4), 251–255. https://doi.org/10.1007/s10230-007-0011-7, 2007

Deák, G. *et al.* (2007) 'Addressing the risk of surface water intrusion in old Romanian salt mines', *Mine Water and the Environment*, 26(4), pp. 251–255. doi: 10.1007/s10230-007-0011-7.

Diakiv, V.: (2012) 'Conformities to the Law of Development of Tekhnogenic Activated Salt Karst in the Process of Submergence of Mines № 8 and № 9 of the «Solotvinsky Saltmine»', in Collection of scientific studies of Lesya Ukrainka Eastern European National University of Voliny - № 9. Nature of Western Polesie and surrounding areas. Lutsk, pp. 69–79. Available at: http://esnuir.eenu.edu.ua/handle/123456789/220, 2012.

Diakiv, V., and Bilonizhka, P.: (2010) 'The characteristics of the geological structure and present day geoecological condition of Solotvyno salt bed', Bulletin of Lviv University, Geology(24), pp. 62–79., Available at: Available at: http://publications.lnu.edu.ua/bulletins/index.php/geology/article/view/3466, 2010

.

Elliott, J. R., Walters, R. J., and Wright, T. J.: (2016) 'The role of space-based observation in understanding and responding to active tectonics and earthquakes', Nature Communications. Nature Publishing Group, 7, pp. 1–16. doi: 10.1038/ncomms13844, 2016

Fattahi, H., Agram, P., and Simons, M.: (2017) 'A Network-Based Enhanced Spectral Diversity Approach for TOPS Time-Series Analysis', IEEE Transactions on Geoscience and Remote Sensing, 55(2), pp. 777–786. doi: 10.1109/TGRS.2016.2614925., 2017

Ferretti, A.: (2014) Satellite InSAR Data. EAGE Publications BV., ISBN 978-9073834712, 2014

Fuhrmann, T., and Garthwaite, M. C.: (2019) 'Resolving Three-Dimensional Surface Motion with InSAR: Constraints from Multi-Geometry Data Fusion, ', Remote Sensing, 11(3), p. 241. doi: 10.3390/rs11030241, 2019.

Gaidin, A.: (2008) 'The effect of technogenic activity on salt karst', Ecology and nature management, (11), pp. 42–54., Available at: http://dspace.nbuv.gov.ua/handle/123456789/14410, 2008

Galve, J. P., Castañeda, C. and Gutiérrez, F.: (2015) 'Railway deformation detected by DInSAR over active sinkholes in the Ebro Valley evaporite karst, Spain', Natural Hazards and Earth System Sciences, 15(11), pp. 2439–2448. doi: 10.5194/nhess-15-2439-2015, 2015

Glushko, V.V., Kruglov S.S. eds.:Tectonic map of the Ukrainian Carpathians. Scale 1:200 00. –Ministry of Geology of the Ukrainian SSR, Ukrainian Geological Prospecting Research Institute. Kyiv. (In Russian), 1986.

Hanssen, R. F.: Radar Interferometry, Springer, Dordrecht, ISBN 978-0-7923-6945-5 https://doi.org/10.1007/0-306-47633-9, 2001

Herenchuk K. I. (ed.): The nature of the Transcarpathian region. Institution of Higher Education, Lviv. (In Ukrainian), 1981

Hanssen, R. F. (2001) Radar Interferometry, Scientific American. doi: 10.1038/scientificamerican0297-46.

Jones, C. E. and Blom, R. G. (2014) 'Bayou Corne, Louisiana, sinkhole: Precursory deformation measured by radar interferometry', *Geology*, 42(2), pp. 111–114. doi: 10.1130/G34972.1.

Kim, J.-W., Lu, Z., Degrandpre, K., Kim, J.-W., Lu, Z., Degrandpre, K.: Kim, J. W. *et al.* (2016) 'Ongoing Deformation of Sinkholes in Wink, Texas, Observed by Time-Series Sentinel-1A SAR Interferometry (Preliminary Results)', Remote Sensing. Multidisciplinary Digital Publishing Institute, 8(4), p. 313. doi: 10.3390/rs8040313, 2016.

Krézsek, C., and Bally, A. W.: (2006) 'The Transylvanian Basin (Romania) and its relation to the Carpathian fold and thrust belt: Insights in gravitational salt tectonics', Marine and Petroleum Geology, 23(4), pp. 405–442. doi: 10.1016/j.marpetgeo.2006.03.003., 2006

Kuzovenko V.V. (ed.): Geologic Map of pre-Quaternary formations; Transcarpathian series M-34-XXXV (Uzhhorod), L-34-V (Satu Mare). Scale 1:200 000. - West Ukrainian Geology (in Russian), 2001

Kyiv State Cartographic Office: Topographic map of Ukraine Scale 1:100 000, maps for Transcarpathia № 144, 145, 163, 164, 165, 182, 183, 184, 201, 202, 203. Kyiv. (In Russian), 2000

Li, Z., Wright, T., Hooper, A., Crippa, P., Gonzalez, P., Walters, R., Parsons, B.: Towards InSAR everywhere, all the time, with Sentinel-1, ISPRS - International Archives of the Photogrammetry, Remote Sensing and Spatial Information Sciences, XLI-B4(July), 763–766. https://doi.org/10.5194/isprsarchives-XLI-B4-763-2016, 2016

Lisowski, M.: Analytical volcano deformation source models. Volcano Deformation, 279–304., https://doi.org/10.1007/978-3-540-49302-0_8, 2007

Li, Z. *et al.* (2016) 'Towards InSAR everywhere, all the time, with Sentinel-1', *International Archives of the Photogrammetry, Remote Sensing and Spatial Information Sciences - ISPRS Archives*, 41(July), pp. 763–766. doi: 10.5194/isprsarchives-XLI-B4-763-2016.

Malinowska, A. A., Witkowski, W. T., Hejmanowski, R., Chang, L., van Leijen, F. J., Hanssen, R. F.: Malinowska, A. A. *et al.* (2019) 'Sinkhole occurrence monitoring over shallow abandoned coal mines with satellite-based persistent scatterer interferometry', Engineering Geology. doi: 10.1016/j.enggeo.2019.105336, 2019.

Manunta, M., De Luca, C., Zinno, I., Casu, F., Manzo, M., Bonano, M., Lanari, R.: The Parallel SBAS Approach for Sentinel-1 Interferometric Wide Swath Deformation Time-Series Generation: Algorithm Description and Products Quality Assessment. IEEE Transactions on Geoscience and Remote Sensing, 57(9), 6259–6281. https://doi.org/10.1109/TGRS.2019.2904912, 2019

Manunta, M. *et al.* (2019) 'The Parallel SBAS Approach for Sentinel-1 Interferometric Wide Swath Deformation Time-Series Generation: Algorithm Description and Products Quality Assessment', *IEEE Transactions on Geoscience and Remote Sensing*. IEEE, PP, pp. 1–23. doi: 10.1109/TGRS.2019.2904912.

Móga, J., Lippman, L., Tombor, E., Fehér, K., Kéri, A., Borsodi, A.: Geomorphological investigation of the Aknaszlatina

saltkarst (Ukraine), Karsztfejlődés, 20, 185–213, 2015

Móga, J., Szabó, J., Gönczy, S., Lippmann, L., Bódai, B.: The study of the dynamically changing landforms of Aknaszlatina saltkarst by field and GIS methods, Karsztfejlődés, (22), 139–161., http://epa.oszk.hu/03100/03192/00022/pdf/EPA03192_karsztfejlodes_2017_22_139-161.pdf, 2017

Móga, J., Gönczi, S., Berghauer, S., Móga, K.: Georesource or geohazard? Past, present and future of the salt mines in Solotvyno, GeoMetodika, 3(2), 5–19. https://doi.org/10.26888/geomet.2019.3.2.1, 2019

Móga, J. *et al.* (2015) 'GEOMORPHOLOGICAL INVESTIGATION OF THE AKNASZLATINA SALTKARST (UKRAINE)', *KARSZTFEJLŐDÉS*, XX, pp. 185–213. doi: 10.17701/15.185-213.

Móga, J. *et al.* (2017) 'THE STUDY OF THE DINAMICALLY CHANGING LANDFORMS OF AKNASZLATINA SALT KARST BY FIELD AND GIS METHODS', *Karsztfejlődés*, (22), pp. 139–161. doi: 10.17701/17.139-161.

Móga, J. *et al.* (2019) 'GEORESOURCE OR GEOHAZARD? PAST, PRESENT AND FUTURE OF THE SALT MINES IN SOLOTVYNO', *GeoMetodika*, 3(2), pp. 5–19. doi: 10.26888/geomet.2019.3.2.1.

Nakapelukh, M., Bubniak, I., Yegorova, T., Murovskaya, A., Gintov, O., Shlapinskyi, V., Vikhot, Y.: Balanced geological cross-section of the outer Ukrainian Carpathians along the pancake profile. Journal of Geodynamics, 108, 13–25., https://doi.org/10.1016/j.jog.2017.05.005, 2017

Nakapelukh, M. *et al.* (2017) 'Balanced geological cross-section of the outer ukrainian carpathians along the pancake profile', *Journal of Geodynamics*, 108, pp. 13–25. doi: 10.1016/j.jog.2017.05.005.

Nof, R. N. *et al.* (2013) 'Sinkhole precursors along the Dead Sea, Israel, revealed by SAR interferometry', *Geology*, 41(9), pp. 1019–1022. doi: 10.1130/G34505.1.

Onencan, A., Meesters, K., and Van de Walle, B.: (2018) 'Methodology for Participatory GIS Risk Mapping and Citizen Science for Solotvyno Salt Mines,', Remote Sensing, 10(11), p. 1828. doi: 10.3390/rs10111828, 2018.

Osmanoğlu, B., Sunar, F., Wdowinski, S., Cabral-Cano, E.: Time series analysis of InSAR data: Methods and trends, ISPRS Journal of Photogrammetry and Remote Sensing, 115, 90–102. https://doi.org/10.1016/j.isprsjprs.2015.10.003, 2016

Okada, Y.: Internal deformation due to shear and tensile faults in a half-space. Bulletin - Seismological Society of America, 82(2), 1018–1040., 1992

Parizzi, A., Gonzalez, F. R., Brcic, R.: A covariance-based approach to merging InSAR and GNSS displacement rate

measurements. Remote Sensing, 12(2). https://doi.org/10.3390/rs12020300, 2020

Pascal, K., Neuberg, J., Rivalta, E.: On precisely modelling surface deformation due to interacting magma chambers and dykes. Geophysical Journal International, 196(1), 253–278. https://doi.org/10.1093/gji/ggt343, 2013

~~Osmanoğlu, B. *et al.* (2016) 'Time series analysis of InSAR data: Methods and trends', *ISPRS Journal of Photogrammetry and Remote Sensing*, 115, pp. 90–102. doi: 10.1016/j.isprsjprs.2015.10.003.~~

Pepe, A. and Calò, F.: ~~(2017) '~~A review of interferometric synthetic aperture RADAR (InSAR) multi-track approaches for the retrieval of Earth's Surface displacements~~'~~, Applied Sciences (Switzerland), ~~p.~~ 1264. doi: 10.3390/app7121264, 2017~~.~~

Reuter, H. I., Nelson, A. D. and Jarvis, A.: ~~(2007) '~~An evaluation of void - filling interpolation methods for SRTM data', International journal of geographical information science. Taylor & Francis, 21(9), ~~pp.~~ 983–1008. doi: 10.1080/13658810601169899, 2007

~~.~~

La Rosa, A., Pagli, C., Molli, G., Casu, F., De Luca, C., Pieroni, A., D'Amato Avanzi, G.: Growth of a sinkhole in a seismic zone of the northern Apennines (Italy). Natural Hazards and Earth System Sciences, 18(9), 2355–2366. https://doi.org/10.5194/nhess-18-2355-2018, 2018

~~La Rosa, A. *et al.* (2018) 'Growth of a sinkhole in a seismic zone of the northern Apennines (Italy)', *Natural Hazards and Earth System Sciences*, 18(9), pp. 2355–2366. doi: 10.5194/nhess-18-2355-2018.~~

Segall, P.: Earthquake and Volcano Deformation, Princtone University Press, ISBN 9780691133027, 2010

Shakin V. A. (ed.): Geological map of the Ukrainian Carpathians Scale 1 : 200 000. – ' UKR NTRA' (In Russian), 1976

Simons, M., ~~and~~ Rosen, P. A.: ~~(2007) '~~Interferometric Synthetic Aperture Radar Geodesy', in *Treatise on Geophysics*. Elsevier B.V., ~~pp.~~ 391–446. Available at: http://ieeexplore.ieee.org/xpls/abs_all.jsp?arnumber=1024984., 2007

Strozzi, T., Teatini, P., Tosi, L., Wegmüller, U.,Werner, C.: Land subsidence of natural transitional environments by satellite radar interferometry on artificial reflectors. Journal of Geophysical Research: Earth Surface, 118(2), 1177–1191. https://doi.org/10.1002/jgrf.20082, 2013

Tyitov, E. M., Mackiv, B. V., Tyitova V. I., Belik T. I.: Geological map of Transcarpathia Scale 1:200 000. Transcarpathian Geological Expedition. (In Russian), 1979

~~Strozzi, T. *et al.* (2013) 'Land subsidence of natural transitional environments by satellite radar interferometry on artificial~~

reflectors', *Journal of Geophysical Research: Earth Surface*, 118(2), pp. 1177–1191. doi: 10.1002/jgrf.20082.

Velasco, V., Sanchez, C., Papoutsis, I., Antoniadi, S., Kontoes, C., Aifantopoulou, D., Paralykidis, S.: Ground deformation mapping and monitoring of salt mines using InSAR technology. Solution Mining Research Institute Fall 2017 Technical Conference, (25-26 September), 1–20., 2017

Velasco, V. *et al.* (2017) 'Ground deformation mapping and monitoring of salt mines using InSAR technology', in *Solution Mining Research Institute Fall 2017 Technical Conference*, pp. 1–20.

Wegmüller, U., Werner, C., Wiesmann, A., Strozzi, T., Kourkouli, P., Frey, O.:Time-series analysis of Sentinel-1 interferometric wide swath data: Techniques and challenges, 2016 IEEE International Geoscience and Remote Sensing Symposium (IGARSS), Beijing, 2016, 3898-3901, doi: 10.1109/IGARSS.2016.7730012., 2016

Wegmuller, U. *et al.* (2016) 'Time-series analysis of Sentinel-1 interferometric wide swath data: Techniques and challenges', in *International Geoscience and Remote Sensing Symposium (IGARSS)*. IEEE, pp. 3898–3901. doi: 10.1109/IGARSS.2016.7730012.

Yague-Martinez, N., Prats-Iraola, P., Rodriguez Gonzalez, F., Brcic, R., Shau, R., Geudtner, D., Bamler, R.: Interferometric Processing of Sentinel-1 TOPS Data. IEEE Transactions on Geoscience and Remote Sensing, 54(4), 2220–2234. https://doi.org/10.1109/TGRS.2015.2497902, 2016

Yague-Martinez, N. *et al.* (2016) 'Interferometric Processing of Sentinel-1 TOPS Data', *IEEE Transactions on Geoscience and Remote Sensing*, 54(4), pp. 2220–2234. doi: 10.1109/TGRS.2015.2497902.

Zechner, E., Dresmann, H., Mocuța, M., Danchiv, A., Huggenberger, P., Scheidler, S., Zlibut, A.: Salt dissolution potential estimated from two-dimensional vertical thermohaline flow and transport modeling along a Transylvanian salt diapir, Romania. *Hydrogeology Journal*, *27*(4), 1245–1256. https://doi.org/10.1007/s10040-018-1912-1, 2019Zechner, E. *et al.* (2019) 'Salt dissolution potential estimated from two-dimensional vertical thermohaline flow and transport modeling along a Transylvanian salt diapir, Romania', *Hydrogeology Journal*. doi: 10.1007/s10040-018-1912-1.

Andreyeva-Grigorovich, A. *et al.* (1997) 'Regional stratigraphic scheme of Neogene formations of the Central Paratethys in the Ukraine', *GEOLOGICA CARPATHICA*, 48(2), pp. 123–136.

Baer, G. *et al.* (2002) 'The lowest place on Earth is subsiding—An InSAR (interferometric synthetic aperture radar) perspective', *Geological Society of America Bulletin*, 114(1), pp. 12–23. doi: 10.1130/0016-7606(2002)114<0012:TLPOEI>2.0.CO;2.

Berardino, P. *et al.* (2002) 'A new algorithm for surface deformation monitoring based on small baseline differential SAR interferograms', *IEEE Transactions on Geoscience and Remote Sensing*, 40(11), pp. 2375–2383. doi: 10.1109/TGRS.2002.803792.

Bosevs'ka, L. (2015) 'Structural and lithological characteristics Salt diapir Transcarpatia', *Journal of Geology, Geography and Geoecology*, 21(3/2). doi: https://doi.org/10.15421/111307.

Bosevs'ka, L. and Khrushchov, D. (2011) 'ENVIRONMENTA EMERGENCY IN SOLOTVINO: CAUSES AND GEOLOGICAL PROBLEMS SOLUTION STRATEGY', *Journal of Geology, Geography and Geoecology*, 19(3/2 SE). doi: https://doi.org/10.15421/111117.

Bukowski, K. and Czapowski, G. (2009) 'Salt geology and mining traditions: Kalush and Stebnyk mines (Fore-Carpathian region, Ukraine)', *Geoturystyka*, 3(18), pp. 27–34.

Bürgmann, R., Rosen, P. A. and Fielding, E. J. (2000) 'Synthetic Aperture Radar Interferometry to Measure Earth's Surface Topography and Its Deformation', *Annual Review of Earth and Planetary Sciences*, 28(1), pp. 169–209. doi: 10.1146/annurev.earth.28.1.169.

CHIŞ, V. T. and KOSINSZKI, S. (2011) 'GEOGRAPHICAL INTRODUCTARY CHARACTERIZATION OF THE UPPER TISA RIVER BASIN (ROMANIA-UKRAINE)', *Transylv. Rev. Syst. Ecol. Res.*, 11(The Upper Tisa River Basin), pp. 1–14.

Cis P.M. 1962: The geomorphology of USSR. – Publishing house of Lviv University. p.244. (In Ukrainian)

Crosetto, M. *et al.* (2016) 'Persistent Scatterer Interferometry: A review', *ISPRS Journal of Photogrammetry and Remote Sensing*. International Society for Photogrammetry and Remote Sensing, Inc. (ISPRS), 115, pp. 78–89. doi: 10.1016/j.isprsjprs.2015.10.011.

Czikhardt, R. *et al.* (2017) 'Ground stability monitoring of undermined and landslide prone areas by means of sentinel-1 multi-temporal InSAR, case study from Slovakia', *Geosciences (Switzerland)*, 7(3), pp. 1–17. doi: 10.3390/geosciences7030087.

Deák, G. *et al.* (2007) 'Addressing the risk of surface water intrusion in old Romanian salt mines', *Mine Water and the Environment*, 26(4), pp. 251–255. doi: 10.1007/s10230-007-0011-7.

Diakiv, V. (2012) 'Conformities to the Law of Development of Tekhnogenic Activated Salt Karst in the Process of Submergence of Mines № 8 and № 9 of the «Solotvinsky Saltmine»', in *Collection of scientific studies of Lesya Ukrainka Eastern European National University of Voliny – № 9. Nature of Western Polesie and surrounding areas*. Lutsk, pp. 69–79. Available at: http://esnuir.eenu.edu.ua/handle/123456789/220.

Diakiv, V. and Bilonizhka, P. (2010) 'The characteristics of the geological structure and present day geoecological condition of Solotvyno salt bed', *Bulletin of Lviv University*, Geology(24), pp. 62–79. Available at: http://publications.lnu.edu.ua/bulletins/index.php/geology/article/view/3466.

Dou, J. *et al.* (2015) 'Automatic detection of sinkhole collapses at finer resolutions using a multi-component remote sensing approach', *Natural Hazards*. Springer Netherlands, 78(2), pp. 1021–1044. doi: 10.1007/s11069-015-1756-0.

Elliott, J. R., Walters, R. J. and Wright, T. J. (2016) 'The role of space-based observation in understanding and responding to active tectonics and earthquakes', *Nature Communications*. Nature Publishing Group, 7, pp. 1–16. doi: 10.1038/ncomms13844.

Fattahi, H., Agram, P. and Simons, M. (2017) 'A Network-Based Enhanced Spectral Diversity Approach for TOPS Time-Series Analysis', *IEEE Transactions on Geoscience and Remote Sensing*, 55(2), pp. 777–786. doi: 10.1109/TGRS.2016.2614925.

Ferretti, A. (2014) *Satellite InSAR Data*. EAGE Publications BV.

Fuhrmann, T. and Garthwaite, M. C. (2019) 'Resolving Three-Dimensional Surface Motion with InSAR: Constraints from Multi-Geometry Data Fusion', *Remote Sensing*, 11(3), p. 241. doi: 10.3390/rs11030241.

Gaidin, A. (2008) 'The effect of technogenic activity on salt karst', *Ecology and nature management*, (11), pp. 42–54. Available at: http://dspace.nbuv.gov.ua/handle/123456789/14410.

Galve, J. P. *et al.* (2008) 'Development and validation of sinkhole susceptibility models in mantled karst settings. A case study from the Ebro valley evaporite karst (NE Spain)', *Engineering Geology*. doi: 10.1016/j.enggeo.2007.11.011.

Galve, J. P., Castañeda, C. and Gutiérrez, F. (2015) 'Railway deformation detected by DInSAR over active sinkholes in the Ebro Valley evaporite karst, Spain', *Natural Hazards and Earth System Sciences*, 15(11), pp. 2439–2448. doi: 10.5194/nhess-15-2439-2015.

Gröger, H. R. *et al.* (2008) 'Tertiary cooling and exhumation history in the Maramures area (internal eastern Carpathians, northern Romania): thermochronology and structural data', *Geological Society, London, Special Publications*, 298(1), pp. 169–195. doi: 10.1144/SP298.9.

Gutiérrez, F. *et al.* (2019) 'Review on sinkhole monitoring and performance of remediation measures by high-precision leveling and terrestrial laser scanner in the salt karst of the Ebro Valley, Spain', *Engineering Geology*. doi: 10.1016/j.enggeo.2018.12.004.

Glushko V.V. – Kruglov S.S. ed. 1986: Tectonic map of the Ukrainian Carpathians. Scale 1:200 00. – Ministry of Geology of the Ukrainian SSR, Ukrainian Geological Prospecting Research Institute. Kyiv. (In Russian).

Hanssen, R. F. (2001) *Radar Interferometry*, *Scientific American*. doi: 10.1038/scientificamerican0297-46.

Herenchuk K. I. (ed.) 1981: The nature of the Transcarpathian region. Institution of Higher Education, Lviv. (In Ukrainian)

IȘTVAN, D. (2011) 'THE GEOLOGICAL STRUCTURE OF THE MARAMUREȘ DEPRESSION', *Transylv. Rev. Syst. Ecol. Res.*, 11(The Upper Tisa River Basin), pp. 15–24.

Jones, C. E. and Blom, R. G. (2014) 'Bayou Corne, Louisiana, sinkhole: Precursory deformation measured by radar interferometry', *Geology*, 42(2), pp. 111–114. doi: 10.1130/G34972.1.

Kim, J. W. *et al.* (2016) 'Ongoing Deformation of Sinkholes in Wink, Texas, Observed by Time-Series Sentinel-1A SAR Interferometry (Preliminary Results)', *Remote Sensing*. Multidisciplinary Digital Publishing Institute, 8(4), p. 313. doi: 10.3390/rs8040313.

Kuzovenko V.V. (ed.) 2001: Geologic Map of pre-Quaternary formations; Transcarpathian series M-34-XXXV (Uzhhorod), L-34-V (Satu Mare). Scale 1:200 000. – West Ukrainian Geology (in Russian).

Kyiv State Cartographic Office 2000: Topographic map of Ukraine Scale 1:100 000, maps for Transcarpathia № 144, 145, 163, 164, 165, 182, 183, 184, 201, 202, 203. Kyiv. (In Russian).

Li, Z. *et al.* (2016) 'Towards InSAR everywhere, all the time, with Sentinel-1', *International Archives of the Photogrammetry, Remote Sensing and Spatial Information Sciences - ISPRS Archives*, 41(July), pp. 763–766. doi: 10.5194/isprsarchives-XLI-B4-763-2016.

Malinowska, A. A. *et al.* (2019) 'Sinkhole occurrence monitoring over shallow abandoned coal mines with satellite-

based persistent scatterer interferometry', *Engineering Geology*. doi: 10.1016/j.enggeo.2019.105336.

Manunta, M. *et al.* (2019) 'The Parallel SBAS Approach for Sentinel-1 Interferometric Wide Swath Deformation Time-Series Generation: Algorithm Description and Products Quality Assessment', *IEEE Transactions on Geoscience and Remote Sensing*. IEEE, PP, pp. 1–23. doi: 10.1109/TGRS.2019.2904912.

Móga, J. *et al.* (2015) 'GEOMORPHOLOGICAL INVESTIGATION OF THE AKNASZLATINA SALTKARST (UKRAINE)', *KARSZTFEJLŐDÉS*, XX, pp. 185–213. doi: 10.17701/15.185-213.

Móga, J. *et al.* (2017) 'THE STUDY OF THE DINAMICALLY CHANGING LANDFORMS OF AKNASZLATINA SALT KARST BY FIELD AND GIS METHODS', *Karsztfejlődés*, (22), pp. 139–161. doi: 10.17701/17.139-161.

Móga, J. *et al.* (2019) 'GEORESOURCE OR GEOHAZARD? PAST, PRESENT AND FUTURE OF THE SALT MINES IN SOLOTVYNO', *GeoMetodika*, 3(2), pp. 5–19. doi: 10.26888/geomet.2019.3.2.1.

Nakapelukh, M. *et al.* (2017) 'Balanced geological cross-section of the outer ukrainian carpathians along the pancake profile', *Journal of Geodynamics*, 108, pp. 13–25. doi: 10.1016/j.jog.2017.05.005.

Nam, B. H. and Shamet, R. (2020) 'A preliminary sinkhole raveling chart', *Engineering Geology*. doi: 10.1016/j.enggeo.2020.105513.

Nof, R. N. *et al.* (2013) 'Sinkhole precursors along the Dead Sea, Israel, revealed by SAR interferometry', *Geology*, 41(9), pp. 1019–1022. doi: 10.1130/G34505.1.

Onencan, A., Meesters, K. and Van de Walle, B. (2018) 'Methodology for Participatory GIS Risk Mapping and Citizen Science for Solotvyno Salt Mines', *Remote Sensing*, 10(11), p. 1828. doi: 10.3390/rs10111828.

Osmanoğlu, B. *et al.* (2016) 'Time series analysis of InSAR data: Methods and trends', *ISPRS Journal of Photogrammetry and Remote Sensing*, 115, pp. 90–102. doi: 10.1016/j.isprsjprs.2015.10.003.

Pepe, A. and Calò, F. (2017) 'A Review of Interferometric Synthetic Aperture RADAR (InSAR) Multi-Track Approaches for the Retrieval of Earth ' s Surface Displacements', pp. 1–40. doi: 10.3390/app7121264.

Perski, Z. *et al.* (2009) 'InSAR analyses of terrain deformation near the Wieliczka Salt Mine, Poland', *Engineering Geology*. Elsevier B.V., 106(1–2), pp. 58–67. doi: 10.1016/j.enggeo.2009.02.014.

Reuter, H. I., Nelson, A. D. and Jarvis, A. (2007) 'An evaluation of void - filling interpolation methods for SRTM data', *International journal of geographical information science*. Taylor & Francis, 21(9), pp. 983–1008. doi: 10.1080/13658810601169899.

La Rosa, A. *et al.* (2018) 'Growth of a sinkhole in a seismic zone of the northern Apennines (Italy)', *Natural Hazards and Earth System Sciences*, 18(9), pp. 2355–2366. doi: 10.5194/nhess-18-2355-2018.

Scotto di Santolo, A., Forte, G. and Santo, A. (2018) 'Analysis of sinkhole triggering mechanisms in the hinterland of Naples (southern Italy)', *Engineering Geology*. doi: 10.1016/j.enggeo.2018.02.014.

Simons, M. and Rosen, P. A. (2007) 'Interferometric Synthetic Aperture Radar Geodesy', in *Treatise on Geophysics*. Elsevier B.V., pp. 391–446. Available at: http://ieeexplore.ieee.org/xpls/abs_all.jsp?arnumber=1024984.

Shakin V. A. (ed.) 1976: Geological map of the Ukrainian Carpathians Scale 1 : 200 000. ' UKR NTRA'

(InRussian).

Ślączka, A. *et al.* (2007) 'Geology and Hydrocarbon Resources of the Outer Carpathians, Poland, Slovakia, and Ukraine: General Geology', *The Carpathians and Their Foreland: Geology and Hydrocarbon Researces: AAPG Memoir 84*, pp. 221–258. doi: 10.1306/985610m843070.

Strozzi, T. *et al.* (2013) 'Land subsidence of natural transitional environments by satellite radar interferometry on artificial reflectors', *Journal of Geophysical Research: Earth Surface*, 118(2), pp. 1177–1191. doi: 10.1002/jgrf.20082.

Szakács, A. and Krézsek, C. (2006) 'Volcano-basement interaction in the Eastern Carpathians: Explaining unusual tectonic features in the Eastern Transylvanian Basin, Romania', *Journal of Volcanology and Geothermal Research*, 158(1–2), pp. 6–20. doi: 10.1016/j.jvolgeores.2006.04.012.

Tischler, M. *et al.* (2007) 'Miocene tectonics of the Maramures area (Northern Romania): implications for the Mid-Hungarian fault zone', *International Journal of Earth Sciences*, 96(3), pp. 473–496. doi: 10.1007/s00531-006-0110-x.

Tyitov E. M. – Mackiv B. V. – Tyitova V. I. – Belik T. I. 1979: Geological map of Transcarpathia Scale 1:200 000. Transcarpathian Geological Expedition. (In Russian).

Valenzuela, P. *et al.* (2015) 'Active sinkholes: A geomorphological impact of the Pajares Tunnels (Cantabrian Range, NW Spain)', *Engineering Geology*, 196, pp. 158–170. doi: 10.1016/j.enggeo.2015.07.007.

Velasco, V. *et al.* (2017) 'Ground deformation mapping and monitoring of salt mines using InSAR technology', in *Solution Mining Research Institute Fall 2017 Technical Conference*, pp. 1–20.

Voznesenski A. I. 1988: The history of formation of neogene sediments in the Transcarpathian troughs. – USSR Academy of Sciences, „Nauka" (Science), Moscow. p.109. (In Russian).

Wegmuller, U. *et al.* (2016) 'Time-series analysis of Sentinel-1 interferometric wide swath data: Techniques and challenges', in *International Geoscience and Remote Sensing Symposium (IGARSS)*. IEEE, pp. 3898–3901. doi: 10.1109/IGARSS.2016.7730012.

Wegnüller, U. *et al.* (2016) 'Sentinel-1 Support in the GAMMA Software', *Procedia Computer Science*. The Author(s), 100, pp. 1305–1312. doi: 10.1016/j.procs.2016.09.246.

Wysocka, A. *et al.* (2016) 'The Middle Miocene of the Fore-Carpathian Basin (Poland, Ukraine and Moldova)', *Acta Geologica Polonica*, 66(3), pp. 351–401. doi: 10.1515/agp-2016-0017.

Yague-Martinez, N. *et al.* (2016) 'Interferometric Processing of Sentinel-1 TOPS Data', *IEEE Transactions on Geoscience and Remote Sensing*, 54(4), pp. 2220–2234. doi: 10.1109/TGRS.2015.2497902.

Zechner, E. *et al.* (2019) 'Salt dissolution potential estimated from two-dimensional vertical thermohaline flow and transport modeling along a Transylvanian salt diapir, Romania', *Hydrogeology Journal*. doi: 10.1007/s10040-018-1912-1.

European Space Agency. Sentinel-1 User Handbook, September 2013: ESA User Guide; GMES-S1OP-EOPG-TN-13-0001; European Space Agency: Paris, France, 2013; p. 80.

Figure 1: Pictures of some sinkholes in the Solotvyno salt mining area (credit: S. Gönczy)

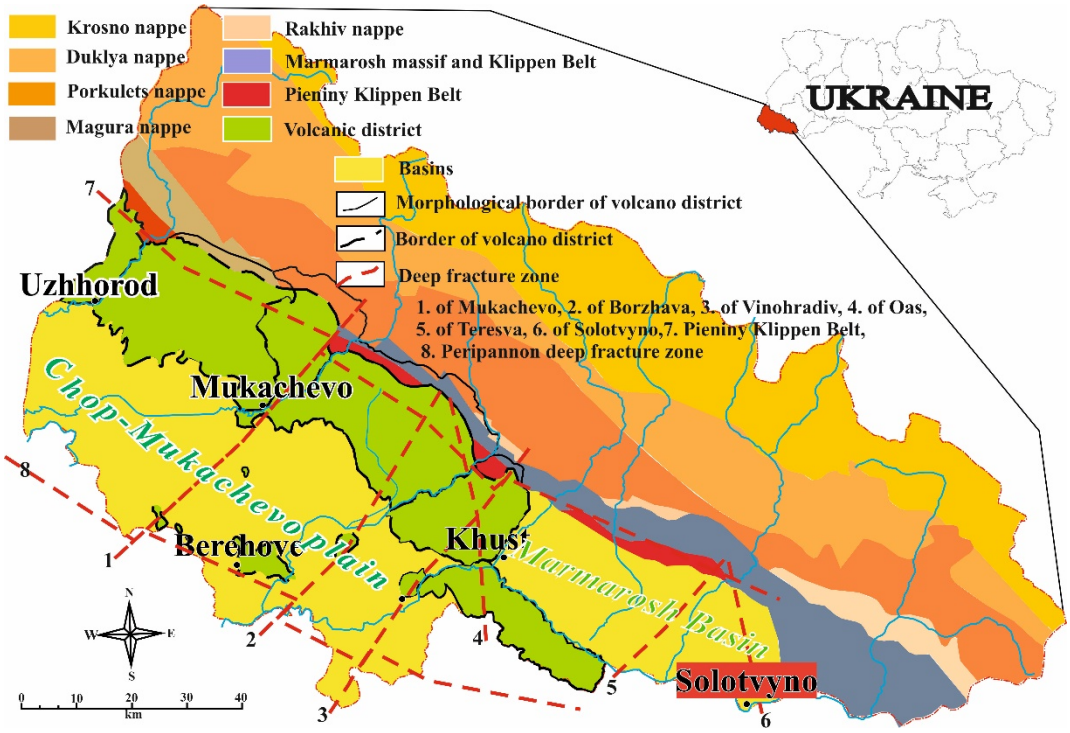

Figure 2: Geological sketch map of the Ukrainian Subcarpathians compiled from © Cis, 1962; © Shakin, 1976; © Tyitov et al. 1979; © Herencsuk (ed.), 1981; © Glusko-Kruglov, 1986; © Kyiv State Cartographic Office 2000; © Kuzovenko (ed.), 2001

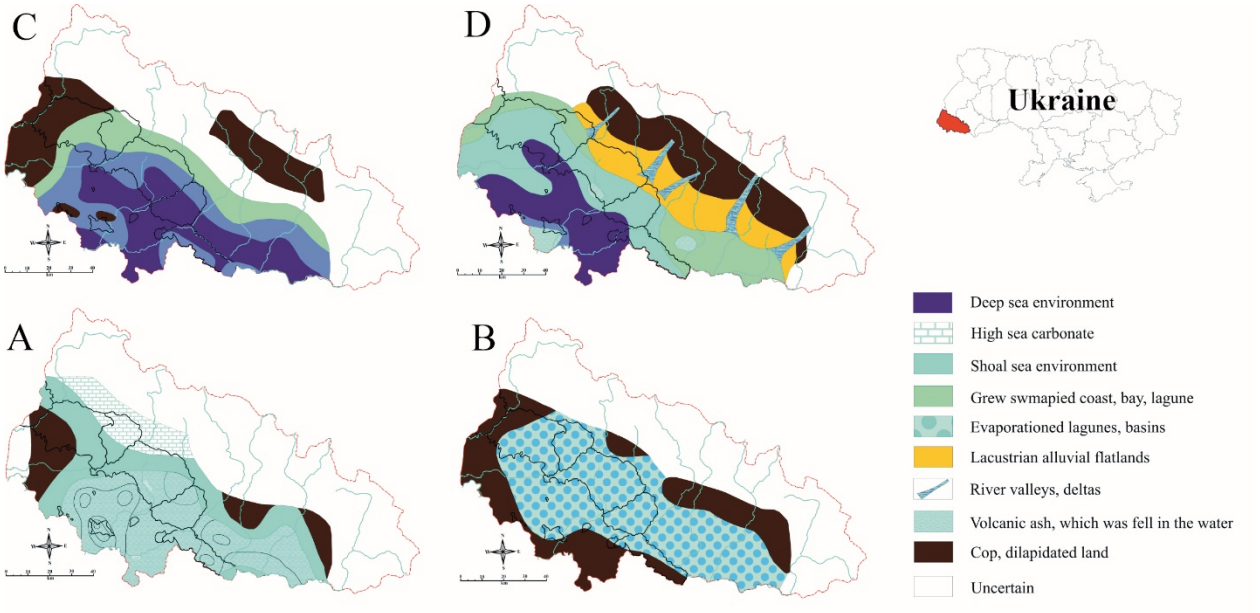

~~**Figure 3: Paleogeographic reconstructions of the Solotvyno Basin in the Carpathian period (a), at the beginning of the Badenian period (b), in the middle Badenian period (c) and at the Badenian-Sarmation boundary (d) (© Voznesenski, 1988)**~~

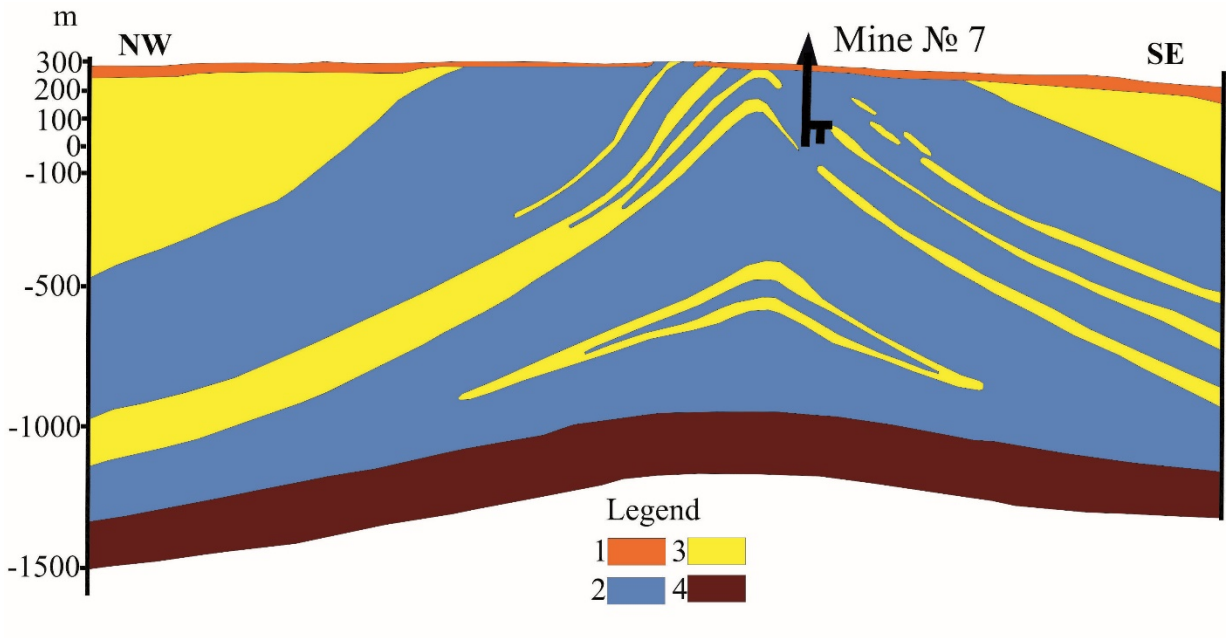

~~**Figure 4: Geological cross section of the Solotvyno salt dome. Legend: 1. fluvial sediments; 2. Tereblya Formation; 3. Solotvyno Formation; 4. Novoselytsa Formation**~~

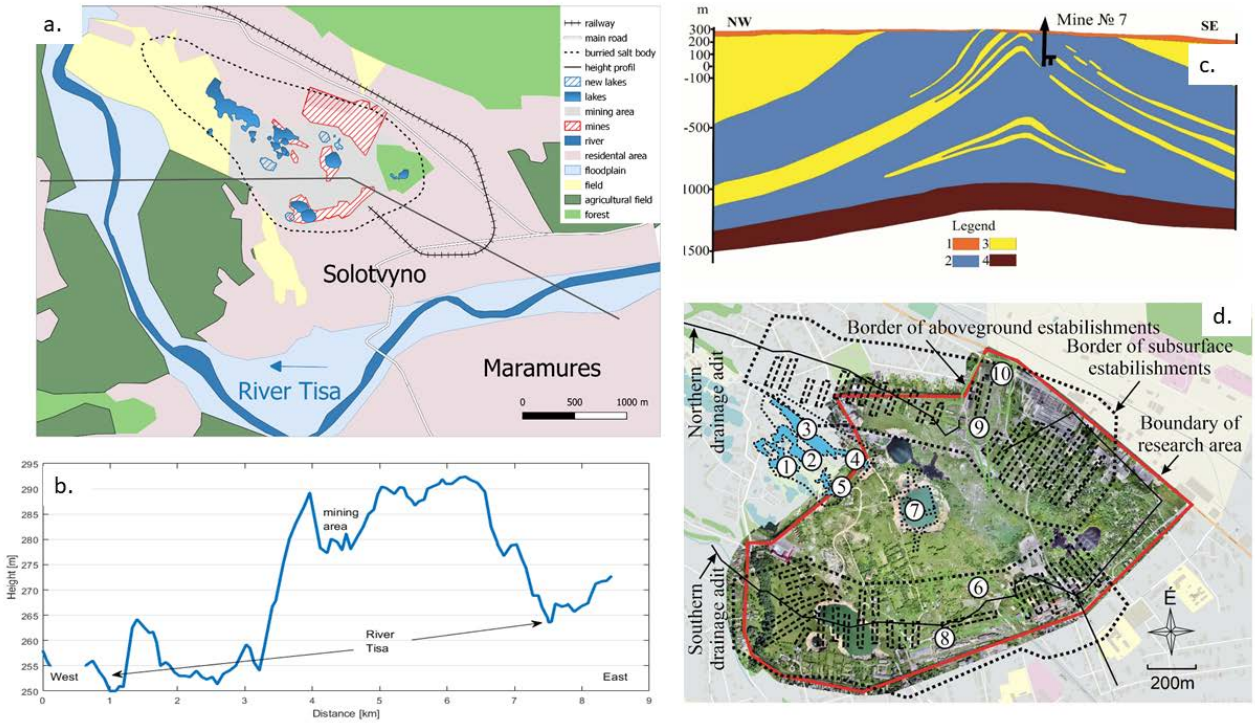

1000

Figure ~~5~~3: The investigated area. | a. Overview map of Solotvyno and its surrounding, showing the approximate location of the salt dome. Lakes with hatch pattern show sinkholes opened after the detailed geomorphological mapping of © Móga et al. 2015. | b. Topographic profile across the section (black line) marked on figure a. | c. Geological cross section of the Solotvyno salt dome. Legend: 1. fluvial sediments; 2. Tereblya Formation; 3. Solotvyno Formation; 4. Novoselytsa Formation | ~~c~~d. Detailed picture of the area with the salt mines shown on a UAV map. 1. Kristina mine; 2. Albert mine; 3. Kunigunda mine; 4. Nicholas mine; 5. Joseph mine; 6. Old Louis mine; 7. Francis mine or mine ~~№~~7th; 8. New Louis mine or mine ~~№~~ 8th; 9th ~~.~~ mine ~~№9~~; 10th ~~.~~ mine ~~№10~~. Lakes are depicted in blueish shades.

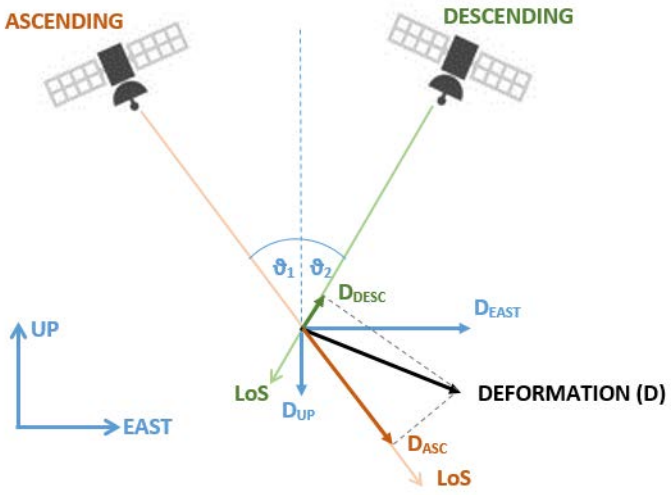

Figure ~~12~~4: Decomposition of the total deformation to ascending and descending ~~LOS~~LOS components as well as to vertical and quasi-horizontal (East-West) components

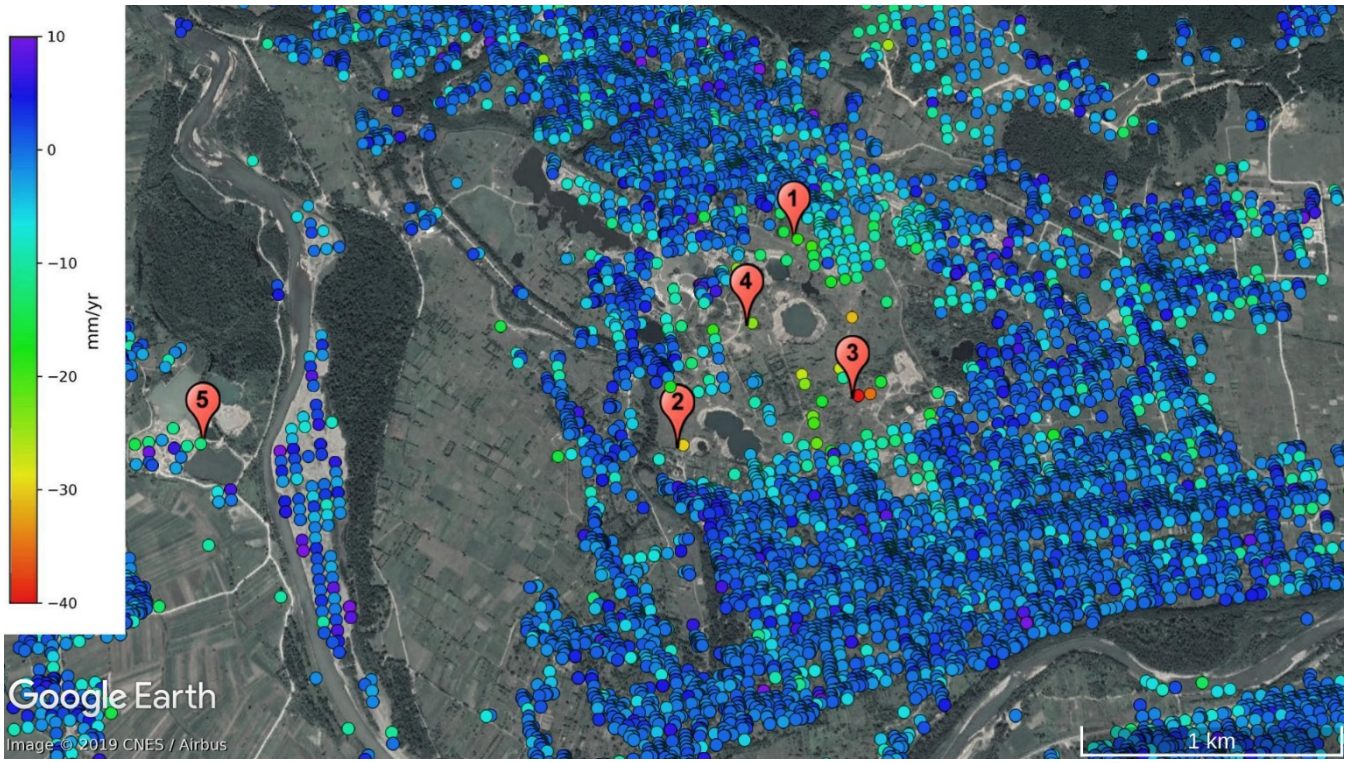

Figure ~~6~~5: Linear rate of line-of-sight deformation from Sentinel-1 ascending pass for the investigated area (see explanation of numbers in the text). Contains modified Copernicus Sentinel data [2014-2019], background © Google.

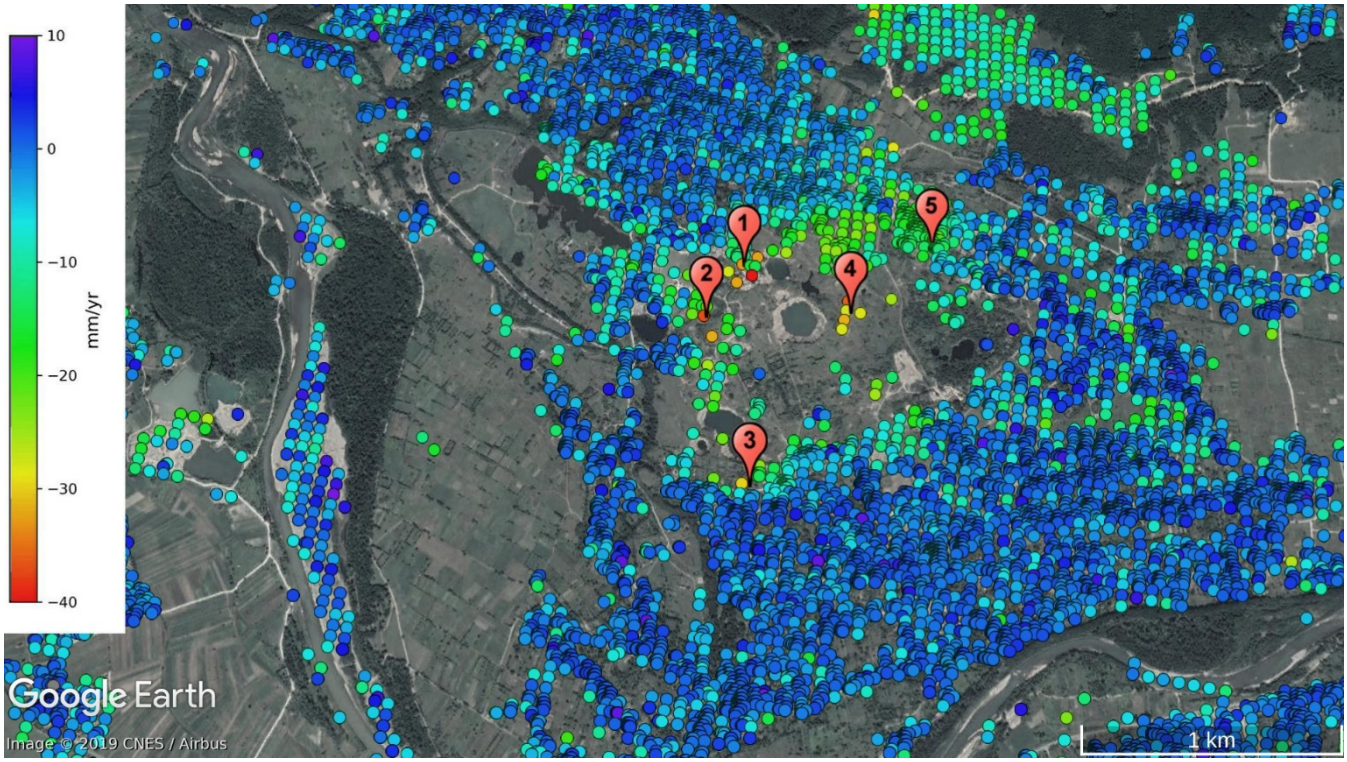

Figure ~~7~~6: Linearly estimated ~~LoS~~LOS deformation rate in mm/yr calculated from Sentinel-1 descending pass data for the investigated area. Contains modified Copernicus Sentinel data [2014-2019], background © Google.

1020

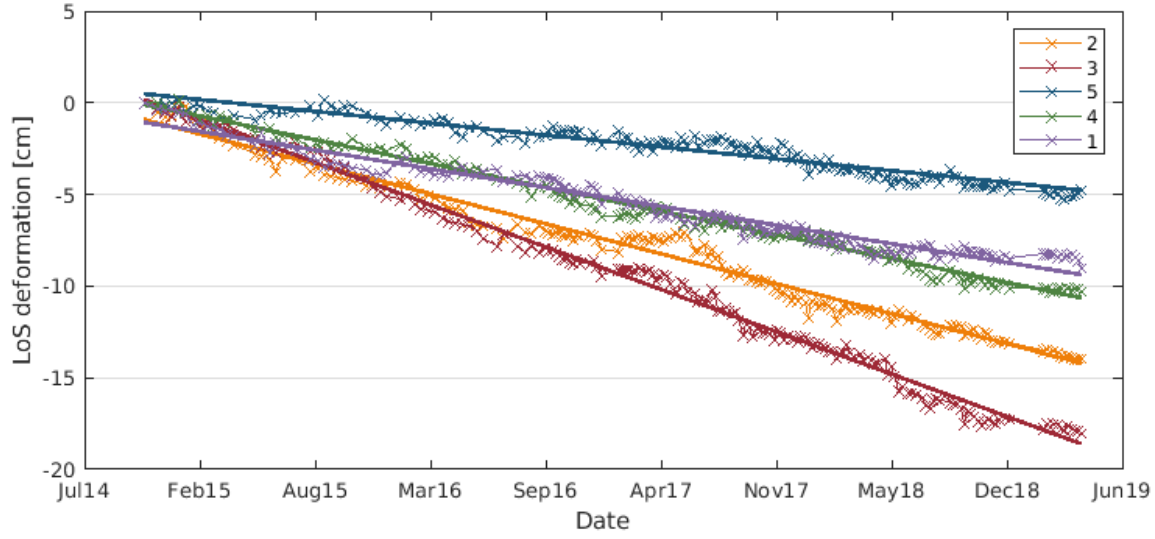

Figure ~~8~~7: ~~LOS~~LOS deformation of some selected points (see Fig ~~6~~5. for location) determined from the ascending scenes

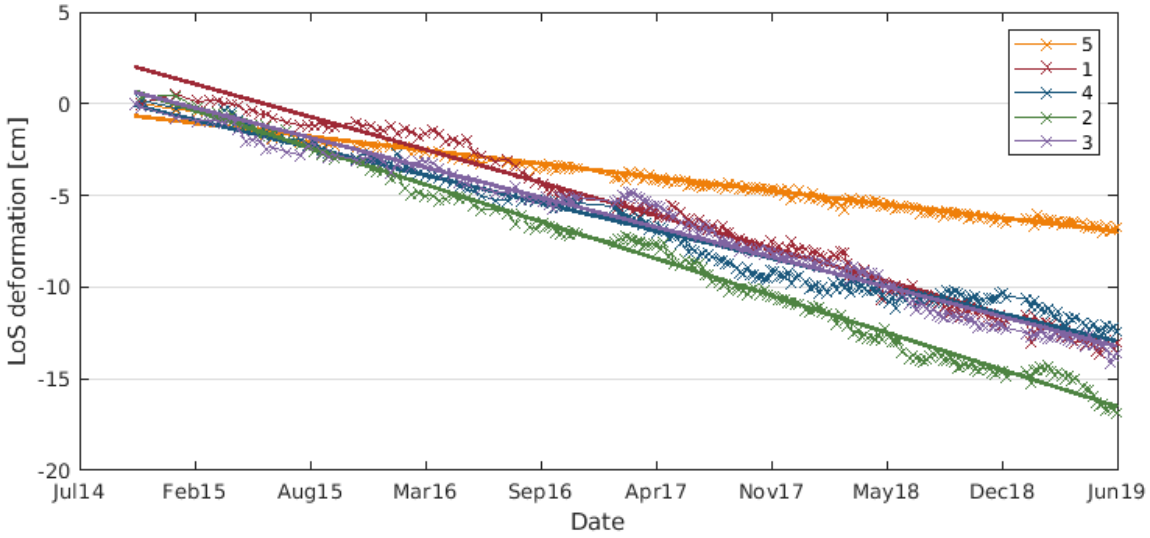

Figure ~~98~~: Time series of some selected points (see Fig. ~~76~~. for location) from the analysis of Sentinel-1 descending scenes

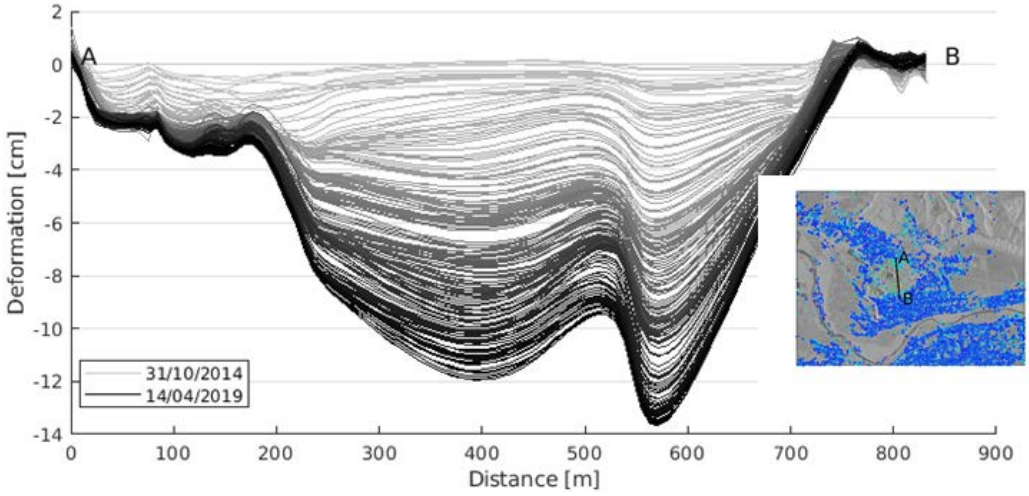

1025

Figure ~~109~~: Temporal evolution of ~~LOS~~LOS surface deformation for the AB cross-section from ascending Sentinel-1 data. For the location of the section see the insert. Shade of grey varies from light to dark as time advances (lightest: October 2014, darkest: April 2019)

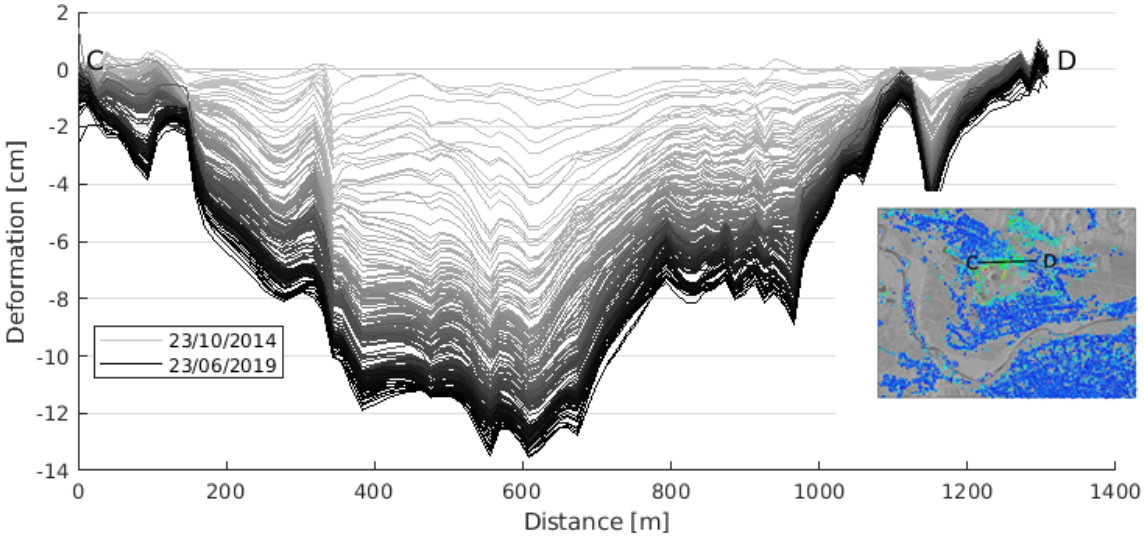

Figure ~~11~~10: Progress of ~~LOS~~LOS surface deformation from descending pass Sentinel-1 data. Location of cross-section is given in the insert. Shade of gray varying from light (October 2014) to dark (June 2016)

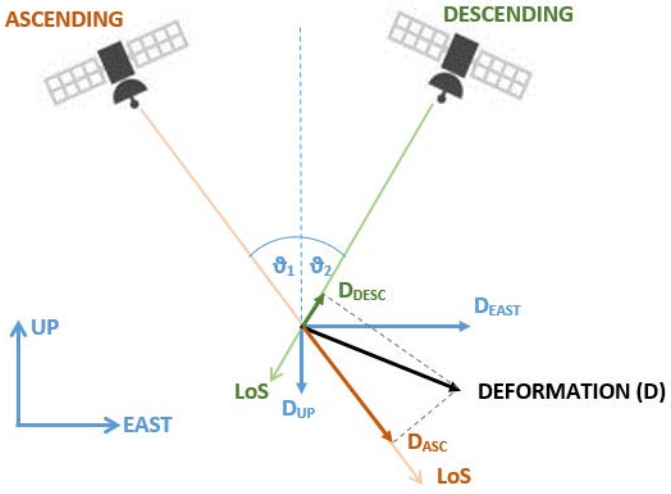

~~**Figure 12: Decomposition of the total deformation to ascending and descending LOS components as well as to vertical and quasi-horizontal (East-West) components**~~

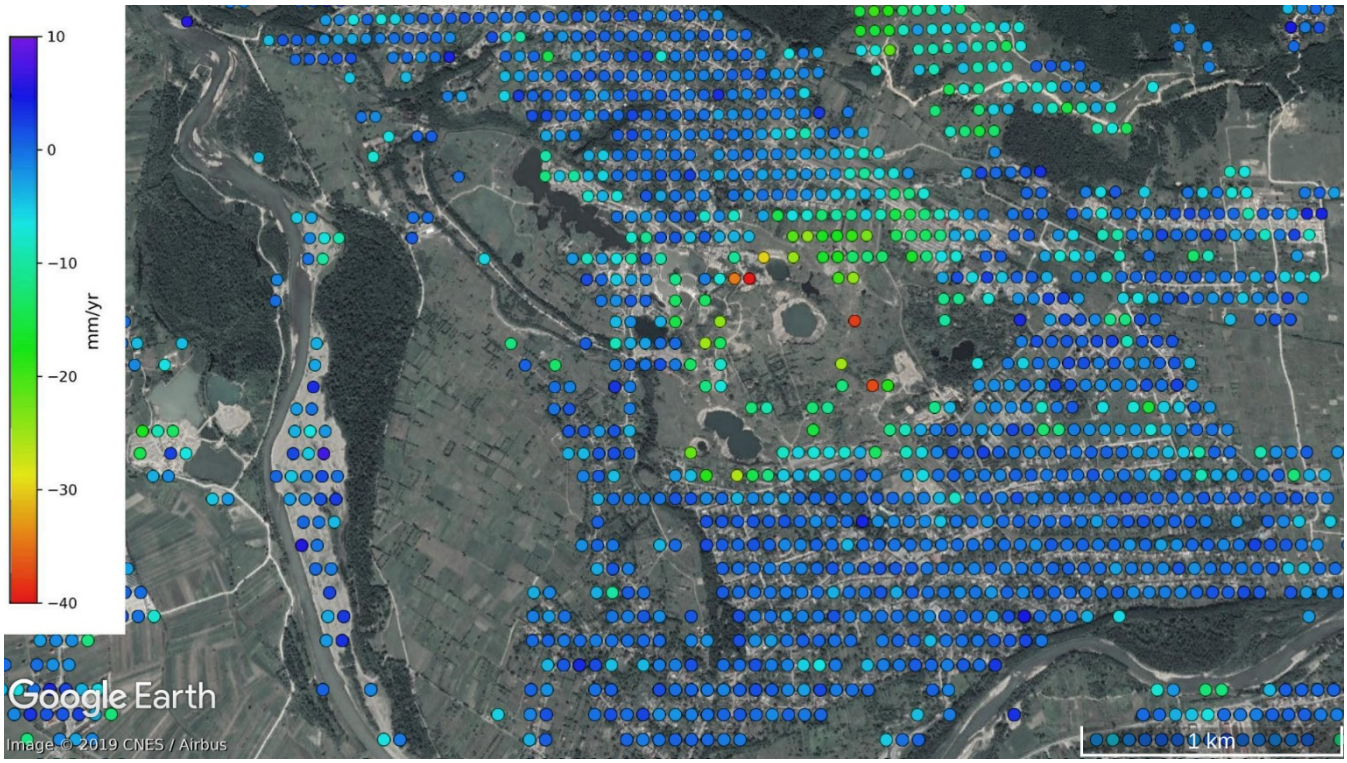

Figure 1~~3~~1: Vertical deformation rate determined from Sentinel-1 data from track 29 and track 80. Contains modified Copernicus Sentinel data [2014-2019], background © Google.

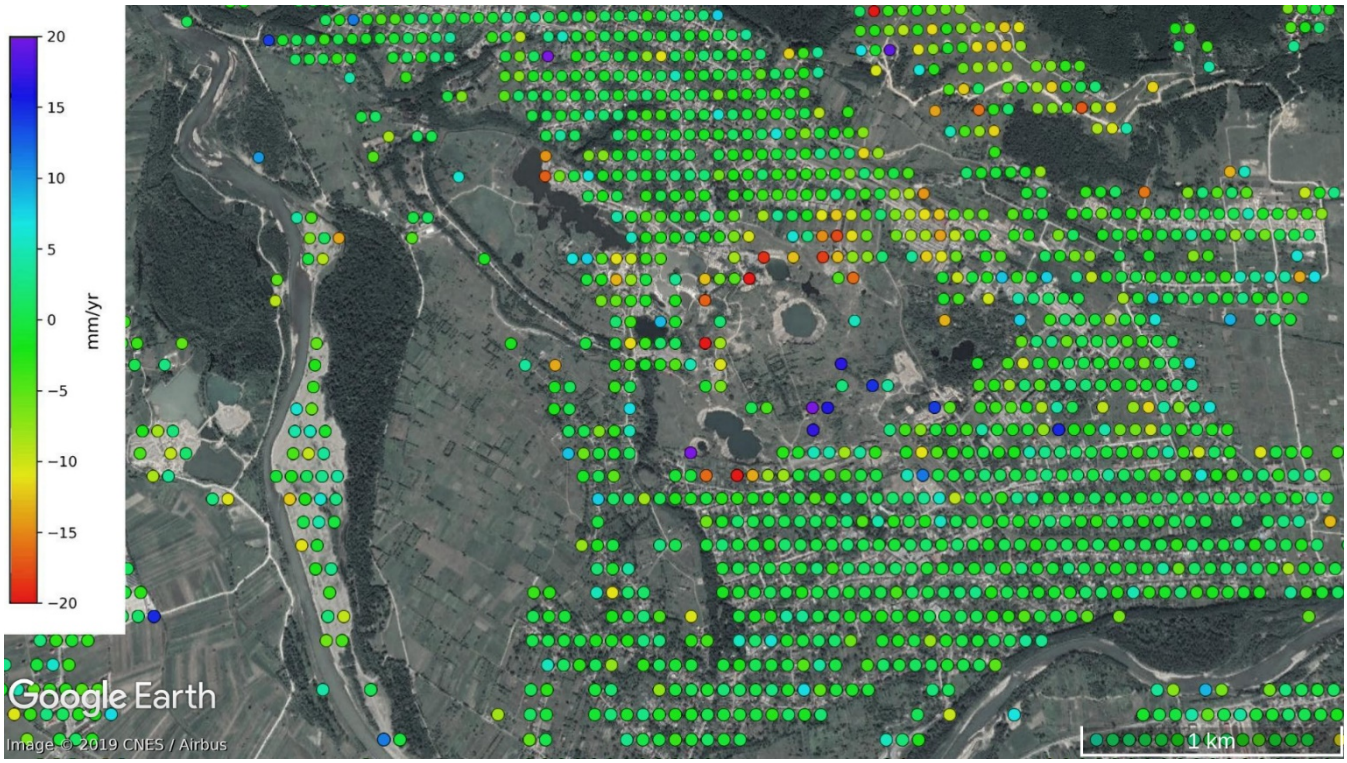

Figure ~~14~~12: East-west (positive in east direction) deformation rate of the area of interest computed from ascending and descending deformation rates. Contains modified Copernicus Sentinel data [2014-2019], background © Google.

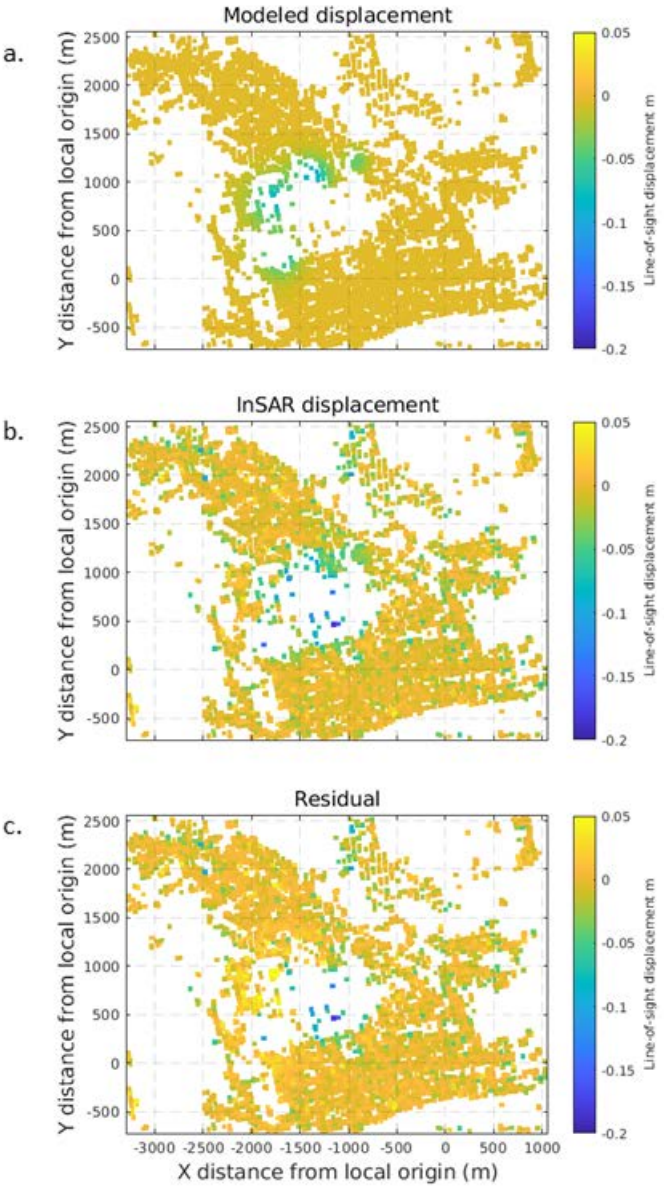

Fig. 13. Cumulative LOS deformation a. computed from the quad-configuration source model, b. deformation from the ascending Sentinel-1 observation and c. residuals after subtracting the best-fitting model

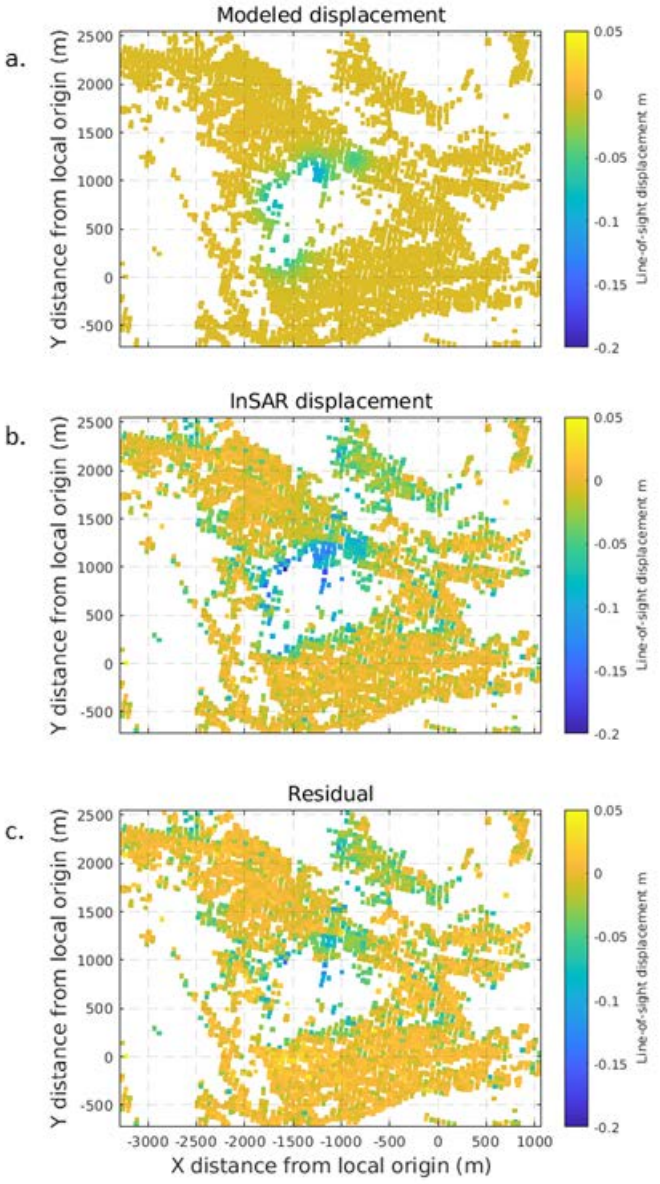

Fig. 14. Cumulative LOS deformation a. of the best-fitting model using four dislocation sources, b. deformation from the descending Sentinel-1 observation and c. residuals after subtracting the modeled displacement from the cumulative deformation

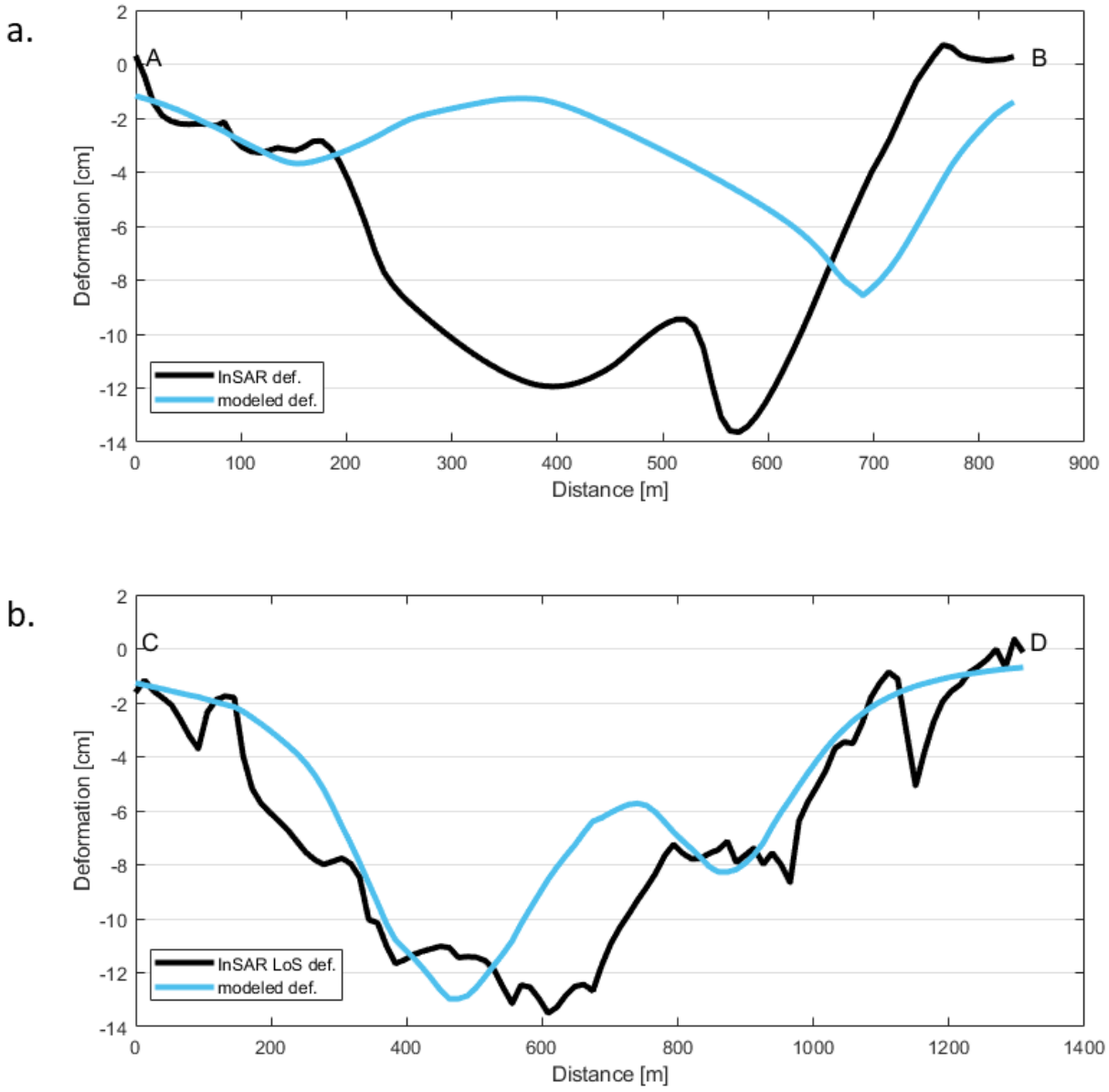

Fig. 15. Observed cumulative LOS and best-fitting model LOS deformations along selected profiles (given on Fig. 9. and 10.) for the ascending (a.) and descending (b.) passes.

	The name of the mine	Start of extraction	Completion of extraction	Cause of the completion of extraction
1	Kristina mine	1778	1781	low quality salt
2	Albert mine	1781	1789	water inrush because the implosLOSion of the surface
3	Kunigunda mine	1789	1905	water inrush because the implosLOSion of the surface
4	Nicholas mine	1789	1905	water inrush because the implosLOSion of the surface
5	Joseph mine	1804	1850	low quality salt, water inrush
6	Old Louis mine	1804	1810	low quality salt
7	Francis mine or mine №7th	1809	1953	water inrush
8	New Louis mine or mine №8th	1886	2007	water inrush
9	mine №9th	1975	2008	water inrush
10	mine №10th	It was made in the end of the eighties, but it has never worked		

Table 1. Summary of mining activity in Solotvyno

Time span	Track	heading	incidence angle	Number of images
20141031 - 20190414	29 (ascending)	-14.6°	41.4°	207
20141023- 20190623	80 (descending)	194.6°	36.3°	211

Table 2. Summary of Sentinel-1 data used in this study

1060

	model #1		model #2		model #3		model #4	
	I	R	I	R	I	R	I	R
length [m]	36	24.1	72.5	63.5	80	78.2	80	72.3
width [m]	42	64.0	176	187.8	80	81.8	90	82.1
depth [m]	180	199.7	222	231.9	280	273.1	295	295.9
strike angle [deg]	5	12.8	21.5	19.1	22	18.7	21	17.1
X center [m]	-870	-880.3	-1195	-1259.1	-1600	-1630.8	-1700	-1700.5
Y center [m]	1160	1195.8	956	1029.6	230	224.9	810	793.1
opening [m]	-3.2	-2.8	-1.4	-1.2	-3.9	-2.3	-3.8	-3.1

Table 3. Analytical model parameters used in the source modeling. "I" refers to initial, "R" to refined values; coordinates are given in local rectangular system, shown on Fig. 13.

1065